Increased prostaglandin-D_2 in male but not female STAT3-deficient hearts shifts cardiac progenitor cells from endothelial to white adipocyte differentiation

Short title: Sex-specific epigenetic priming of progenitor cells in heart-failure

Elisabeth Stelling[1§], Melanie Ricke-Hoch[1§], Sergej Erschow[1], Steve Hoffmann[2], Anke Katharina Bergmann[3], Maren Heimerl[1], Stefan Pietzsch[1], Karin Battmer[6], Alexandra Haase[4], Britta Stapel[1,5#], Michaela Scherr[6], Jean-Luc Balligand[7], Ofer Binah[8], Denise Hilfiker-Kleiner[1*]

[1]Department of Cardiology and Angiology, Hannover Medical School, Hannover, Germany

[2]Computational Biology, Leibniz Institute on Aging, Jena, Germany

[3]Department of Human Genetics, Hannover Medical School, Hannover, Germany

[4]Leibniz Research Laboratories for Biotechnology and Artificial Organs (LEBAO), Department of Cardiothoracic, Transplantation and Vascular Surgery, Hannover Medical School, Hannover, Germany

[5#]current address: Department of Psychiatry, Social Psychiatry and Psychotherapy, Hannover Medical School, Hannover, Germany

[6]Department of Hematology, Hemostasis, Oncology and Stem Cell Transplantation, Hannover Medical School, Hannover, Germany

[7]Pole of Pharmacology, Institut de Recherche Expérimentale et Clinique, Université catholique de Louvain, Brussels, Belgium

[8]Department of Physiology, Biophysics and Systems Biology, Ruth and Bruce Rappaport Faculty of Medicine and Research Institute, Technion – Israel Institute of Technology, Haifa, Israel

*Corresponding author:

E-mail: hilfiker.denise@mh-hannover.de (DH-K)

[§]These authors contributed equally to this work.

Abstract

Cardiac levels of the signal transducer and activator of transcription factor-3 (STAT3) decline with age, and male but not female mice with a cardiomyocyte-specific STAT3 deficiency (CKO) display premature age-related heart failure associated with reduced cardiac capillary density. In the present study isolated male and female CKO-cardiomyocytes exhibit increased prostaglandin (PG)-generating cyclooxygenase-2 (COX-2) expression. The PG-degrading hydroxyprostaglandin-dehydrogenase-15 (HPGD) expression is only reduced in male cardiomyocytes, which is associated with increased PGD_2 secretion from isolated male but not female CKO-cardiomyocytes. Reduced HPGD expression in male cardiomyocytes derive from impaired androgen-receptor-(AR)-signaling due to loss of its co-factor STAT3. Elevated PGD_2 secretion in males is associated with increased white adipocyte accumulation in aged male but not female hearts. Adipocyte differentiation is enhanced in isolated SCA-1^+-cardiac-progenitor-cells (CPC) from young male CKO-mice compared to the adipocyte differentiation of male wildtype (WT)-CPC and CPC isolated from female mice. Epigenetic analysis in freshly isolated male CKO-CPC display hypermethylation in pro-angiogenic genes (*Fgfr2*, *Epas1*) and hypomethylation in the white adipocyte differentiation gene *Zfp423* associated with upregulated ZFP423 expression and a shift from endothelial to white adipocyte differentiation compared to WT-CPC. The expression of the histone-methyltransferase EZH2 is reduced in male CKO-CPC compared to male WT-CPC whereas no differences in the EZH2 expression in female CPC were observed. Clonally expanded CPC can differentiate into endothelial cells or into adipocytes depending on the differentiation conditions. ZFP423 overexpression is sufficient to induce white adipocyte differentiation of clonal CPC. In isolated WT-CPC, PGD_2 stimulation reduces the expression of EZH2 thereby upregulating ZFP423 expression and promoting white adipocyte differentiation.

Thus, cardiomyocyte STAT3-deficiency leads to age-related and sex-specific cardiac remodeling and failure in part due to sex-specific alterations in PGD_2 secretion and subsequent epigenetic impairment of the differentiation potential of CPC. Causally involved is the impaired

57 AR signaling in absence of STAT3, which reduces the expression of the PG degrading enzyme

58 HPGD.

59

Introduction

Men and women experience quite different cardiovascular disease susceptibility profiles and outcome, a feature that is poorly understood. Further, the effects of biologic sex on health, disease susceptibility and mortality are vastly understudied (1, 2). Recent studies showed that genetics contribute to sex-specific differences in fat tissue and cardiovascular and metabolic diseases (3). Pathophysiologically enhanced cardiac fat content is frequently observed in patients with heart failure, in arrhythmogenic right ventricular dysplasia (ARVD), and after myocardial infarction (4-6). In patients with dilated cardiomyopathy (DCM), increased fat deposits are associated with more severe left ventricular (LV) dilatation and decreased systolic LV function, compared with DCM patients without enhanced cardiac fat (6). Three different types of fat tissue exist of which brown adipose tissue (BAT), mostly present in embryonic and fetal stages, and beige adipose tissue (BET) present postnatally, utilize glucose and lipids to generate heat and are associated with improved cardiometabolic health (7). Brown and beige adipocytes harbor many similar properties, including multilocular lipid droplets, dense mitochondria, and the activation of a thermogenic gene program involving the PR domain containing 16 (PRDM16) protein. PRDM16 is a transcriptional coregulator that controls the development of brown and beige adipocytes and leads to the upregulation of uncoupling protein 1 (UCP1), a hallmark of BAT/BET (8, 9). The third fat type is defined as white adipose tissue (WAT) which stores energy by accumulating fat droplets. WAT is needed as mechanical protection for organs and secretes cytokines and hormones. Extensive WAT formation is associated with an increased cardiovascular risk as it promotes inflammation and alters the immune-endocrine response (10). WAT-specific gene programs typically upregulate the zinc-finger protein 423 gene (*Zfp423*, the murine ortholog of the human *Znf423*). ZFP423 suppresses the PRDM16-mediated thermogenic program and thereby prevents fat cells from burning energy by keeping white fat cells in an energy-storing state (11). A change in the proportions of adipose tissues occurs with aging, leading to a decline of BAT/BET and an increase in WAT, which plays a central role in cardiovascular diseases and type II diabetes (10, 12). Development, maintenance, and activation of the different adipose tissues are guided

by genetic factors and epigenetic programs, which regulate the *de novo* differentiation of adipocytes from progenitor cells, as well as white-to-brown adipocyte transdifferentiation (7). However, little is known about mechanisms driving the build-up of different fat types in the heart, especially under pathophysiological conditions and whether there are sex-specific differences in these processes.

The cardiac expression and activation of the signal transducer and activator of transcription factor-3 (STAT3) diminishes with age and is notably reduced in failing hearts from patients with dilatative cardiomyopathy (DCM) or peripartum cardiomyopathy (PPCM) (13-16). Moreover, cardiomyocyte-specific deficiency of STAT3 (CKO) leads to age-related heart failure and more pronounced cardiac damage and failure in response to ischemic injury and infection in male mice (17-19). Nulli-pari CKO females seem protected from age-related heart failure but develop PPCM after breeding (14). Beside direct protective effects on cardiomyocytes, cardiomyocyte STAT3 influences also the cardiac cell-to-cell communication by regulating the expression and secretion of paracrine factors, impacting on endothelial cells, fibroblasts, inflammatory cells and endogenous stem cell antigen (SCA)-1^{+} cardiac-progenitor-cells (CPC) (17, 20-23).

The present study shows that cardiomyocyte-specific STAT3 deficiency leads to an upregulation of cyclooxygenase-2 (COX-2, also known as prostaglandinsynthase-2, PGHS-2) in young male and female CKO mice thereby promoting the production of the prostaglandin D_2 (PGD_2) from arachidonic acid. In males, the prostaglandin degrading enzyme hydroxyprostaglandin-dehydrogenase-15 (HPGD) expression is under the control of the androgen receptor (AR) for which STAT3 acts as a co-factor (24). As a consequence, PGD_2 secretion from male CKO-CM but not from female CKO-CM is increased which subsequently represses the Enhancer of Zeste homolog 2 (EZH2) subunit of the Polycomb repressive complexe 2 (PRC2), a histone methyltransferase associated with transcriptional repression of the white adipocyte differentiation factor ZFP423 (25). In turn, EPO, which is also reduced in CKO hearts, has been shown to enhance endothelial differentiation from CKO-CPC (22) and the present study shows that it suppresses the ZFP423 expression and white adipocyte

116 differentiation from CKO-CPC.

117 In summary, STAT3-deficiency leads to sex-specific alterations in the cardiomyocyte
118 secretome which provokes an epigenetic shift in CPC from endothelial cells towards white
119 adipocytes differentiation in male but not female CKO hearts. This process contributes to a
120 decline in capillaries and an increase in WAT deposits with cardiac remodeling and heart
121 failure in aging male but not female CKO mice.

122

Results

Male but not female CKO mice develop age-related heart failure with increased intraventricular fat accumulation and enhanced inflammation and fibrosis

We previously showed that male and female mice with a cardiomyocyte-specific STAT3 deficiency (αMHC-Cre$^{tg/+}$; STAT3$^{flox/flox}$, CKO) exhibit normal cardiac function and morphology at young age (3 months) and that male but not female mice develop left ventricular (LV) systolic dysfunction at 6 months of age (S1 Table and S2 Table) (14, 17). Histological analyses (Oil Red O and Perilipin staining) revealed that LV adipocyte content was low with no difference between WT and CKO mice of both sexes at the age of 3-4 months (Figs 1A and 1B, S1A Fig). At 6-months, however, LVs from male but not female CKO mice displayed increased adipocytes content compared to age- and sex-matched controls (Figs 1A and 1B, S1A Fig). Further analyses revealed positive staining for the adipocyte marker Perilipin and the white adipocyte marker Resistin while the brown/beige adipocyte marker UCP1 could not be detected (Fig 1C, S1B Fig). In addition, the triglyceride content was higher in LV tissue from 6-month-old male CKO hearts compared to age-matched male WT hearts (Fig 1D). Aged male CKO hearts displayed reduced capillary density, elevated numbers of inflammatory cells (CD45 positive infiltrates), increased expression of the monocyte/macrophage marker ADGRE1 and increased fibrosis compared with hearts from age-matched male WT mice (Figs 1E-1H).

COX-2 expression is increased in male and female CKO cardiomyocytes but reduced HPGD expression and increased PGD_2 secretion are only present in male cardiomyocytes

Prostaglandins are metabolites of the arachidonic pathway in which COX-1 and COX-2 and HPGD are rate limiting enzymes. LV tissue from 3- and 6-month-old CKO male mice expressed less HPGD than WT male mice (Fig 2A, S2A Fig) while no such difference was visible between CKO- and WT female mice (S2B and S2C Figs). Moreover, HPGD expression was also lower in male CKO- compared to male WT-CM (Fig 2B) while female CKO- and WT-CM showed no

151 difference (S2D Fig).

152 Increased COX-2 expression was observed in LV tissue of 3- and 6-month-old male and
153 female CKO mice and in isolated male and female cardiomyocytes from young (3-month-old)
154 CKO mice compared to respective sex- and age-matched WT controls (Figs 2C and 2D, S2E-
155 H Figs). PGD_2 levels were increased in the supernatants of male CKO-CM compared to levels
156 in the supernatants of male WT-CM (Fig 2E). Female CKO-CM displayed no differences in
157 secreted PGD_2 levels compared to female WT-CM (S2I Fig).

158

159 **Testosterone-induced expression of HPGD is attenuated in STAT3-knockdown HL-1**
160 **cardiomyocytes**

161 It has been reported that HPGD is positively regulated by the androgen receptor (AR) (26) and
162 that the AR is expressed by HL-1 cardiomyocytes (27). We observed that HPGD expression
163 was significantly lower in control HL-1-STAT3-KD-CM compared to HL-1-ctrl-CM (Figs 2F and
164 2H). Testosterone stimulation markedly induced HPGD in HL-1-ctrl-CM (+68±16%), which was
165 attenuated in HL-1-STAT3-KD-CM (+29±9%) (Fig 2F). In turn, COX-2 was higher in HL-1-
166 STAT3-KD-CM without an additional effect of testosterone treatment compared to HL-1-ctrl-
167 CM (Fig 2G). Treatment with estrogen did not influence HPGD or COX-2 expression of HL-1-
168 ctrl- or HL-1-STAT3-KD-CM (S2J and S2K Figs).

169

170 **PGD_2 promotes white adipocyte differentiation of WT-CPC and of human induced**
171 **pluripotent stem cells**

172 PGD_2 upregulated white adipocyte differentiation in WT-CPC as shown by increased Oil Red
173 O positive cells, which was associated with an early reduction of the Enhancer of Zeste
174 homolog 2 (EZH2) subunit of the Polycomb repressive complex 2 (PRC2), a histone
175 methyltransferase associated with transcriptional repression of the white adipocyte
176 differentiation factor ZFP423 (25) and enhanced ZFP423 expression (Figs 3A-3D). PGD_2 also
177 enhanced expression levels of the adipocyte markers PPARγ, CCAAT enhancer binding
178 protein alpha (CEBPA) and fatty acid binding protein 4 (FABP4) and of the WAT markers

ZFP423, lysozyme 2 (LYZ2) and Resistin, while the expression of BAT/BET markers (EBF transcription factor-2, EBF2 and transmembrane protein 26, TMEM26) remained unchanged (Figs 3E-3L) and PR domain containing 16 (PRDM16) and uncoupling protein 1 (UCP1) expression was not detectable. PGD_2 treatment induced also white adipocyte differentiation in human induced pluripotent stem cells (iPSC) as shown by Oil Red O and Resistin positive cells (S3A Fig). In addition, ZNF423 and CEBPA expression were elevated and EZH2 expression was reduced in PGD_2 treated human iPSC compared to control iPSC (S3B-S3D Figs).

CPC isolated from young male CKO mice display increased adipocyte differentiation potential compared with CPC isolated from young male WT mice

Based on the higher secretion of PGD_2 from male CKO-CM and the effect of PGD_2 on CPC from WT mice (WT-CPC), we evaluated the differentiation potential of freshly isolated CPC from young WT and CKO male mice for which we previously showed that STAT3 is exclusively deleted in cardiomyocytes of CKO mice, while its expression is comparable in CPC from CKO (CKO-CPC) and WT mice (22). CPC showed marked expression of platelet-derived growth factor receptor (PDGFR)α indicative for their mesenchymal stem cell character (Fig 4A and 4B). The lack of preadipocyte factor 1 (PREF-1, highly expressed in the preadipocyte cell line 3T3-L1) expression in CPC confirms that isolated CPC were not contaminated with preadipocytes (Figs 4A and 4B). *In vitro* cultivation led to spontaneous differentiation into various cell types including endothelial cells and adipocytes, as shown previously (22) (Figs 4C and 4D). The spontaneous adipocyte differentiation was 2-fold higher in male CKO-CPC compared with male WT-CPC, despite identical cultivation conditions (Figs 4D and 4E), while no elevated adipocyte differentiation was observed in female WT-CPC and CKO-CPC. After differentiation, male CKO-CPC displayed an upregulation of the general adipocyte markers CEBPA and FABP4 (Figs 4F and 4G), and WAT markers ZFP423, LYZ2 and Resistin (Figs 4H-4J). The expression of the BAT/BET markers EBF2 and TMEM26 was similar in CKO- and WT-CPC (Figs 4K and 4L) and the BAT/BET markers PRDM16 and UCP1 could not be detected.

The epigenetic signature of freshly isolated CPC isolated from young CKO males differs from CPC isolated from young WT males

Since adipocyte priming of CKO-CPC was maintained during *in vitro* cultivation, we analyzed the epigenetic profiles of CKO-CPC and WT-CPC freshly isolated from 3-month-old male mice with normal cardiac function (S1 Table). A genome-wide exploratory methylation profiling by RRBS, revealed a total of 83 differentially methylated regions (DMRs) overlapping with 81 unique genes with a minimum group methylation difference of 0.1 and $p<0.001$ (S4A Fig). DMRs with hypermethylated regions were detected in genes such as *Epas1* and *Fgfr2*, both known to promote angiogenesis (28, 29) (S4A Fig, Figs 5A and 5B). In turn, regions in the vicinity of the *Zfp423* 5-UTR (in exon 2, chr8: 87783293-87783352, Wilcoxon $p<5.5e-6$) were hypomethylated in CKO-CPC compared with WT-CPC (S4A Fig, Fig 5C). *Zfp423* expression is negatively regulated by zinc finger protein 521 (ZFP521) (30), which was slightly hypermethylated in CKO-CPC (Wilcoxon $p<0.02$, S4A Fig, Fig 5D). QRT-PCR confirmed higher mRNA expression of ZFP423 in CKO-CPC compared with WT-CPC, while no difference was observed for ZFP521 expression (Figs 5E and 5F). *Zfp423* expression can also be regulated by bone morphogenetic protein (BMP)2 and BMP4 (30, 31), but no differences were detected in the methylation pattern of these genes and the expression of BMP2 and BMP-4 in LV heart tissue taken from CKO and WT male mice was similar (Figs 5G and 5H). EZH2 expression was reduced in freshly isolated CKO-CPC compared with WT-CPC from male mice (Fig 5I). In turn, no alteration in EZH2 or ZFP423 mRNA levels were observed in CKO- and WT-CPC isolated from 3-month-old female mice (Figs 5J and 5K).

Clonally expanded CPC have the potential to differentiate into endothelial cells and white adipocytes

As freshly isolated CPC are generally a heterogenic pool of cells (22), two clonally expanded CPC cell lines (cCPC) (22, 32) were tested regarding their potential to differentiate into endothelial cells and adipocytes. We observed that the same passage of cCPC cell lines

differentiate into endothelial cells on Matrigel (22, 32) or into adipocytes when adipocyte differentiation media and the peroxisome proliferator activated receptor γ (PPARγ) activator indomethacin (33) were added (S5A and S5B Figs). Adipocyte differentiation led to a reduction in SCA-1 and PDGFRα expression and an upregulation of the general adipocyte markers CEBPA and FABP4 (S5C-S5F Figs). Further analyses showed upregulation of the WAT markers LYZ2, and Resistin while the expression of the BAT/BET markers EBF2 and TMEM26 remained unchanged (S5G-S5J Figs) and PRDM16 and UCP1 were undetectable. Retroviral overexpression of ZFP423 induced white adipocyte differentiation in cCPC as shown by increased Oil Red O staining and enhanced expression of PPARγ2, CEBPA, LYZ2 and Resistin (Figs 6A-6G). The expression of the BAT/BET markers EBF2 and TMEM26 remained unchanged (Figs 6H and 6I) and PRDM16 and UCP1 were not detectable.

EPO reduces ZFP423 expression and adipocyte differentiation of CKO-CPC

We previously demonstrated that the addition of recombinant murine (rm)EPO to CKO-CPC cultures restored their endothelial differentiation potential (22). Here, we observed that addition of rmEPO to CKO-cultures persistently reduced the ZFP423 expression in CKO-CPC (S6A and S6B Figs), which was associated with attenuated adipocyte differentiation, as shown by reduced Oil Red O positive cells and reduced expression of CEBPA and FABP4 (S6C-S6F Figs). However, addition of rmEPO to isolated CPC for 48 h had no effect on EZH2 expression (S6G Fig).

LV tissue from male patients with end-stage heart failure due to DCM/ICM display higher cardiac CEBPA expression and lower HPGD expression compared with non-failing LV samples from healthy male organ donors

We previously showed that STAT3 is reduced in hearts from patients with end-stage heart failure (15). Here, we observed that LV tissue from male patients with end-stage heart failure due to DCM or ischemic cardiomyopathy (ICM) (n=8) displayed higher CEBPA (+133±142%, $P<0.05$) and a non-significant trend to higher COX-2 (+33±91%, n.s.) expression compared

263 with LV samples from healthy male organ donors (n=6). In addition, HPGD mRNA levels were
264 significantly lower in male failing LV samples (-55±12%, P<0.05) compared with LV samples
265 from healthy male organ donors.

Discussion

We previously reported that cardiomyocyte-specific STAT3-deficiency in male but not female mice leads to age-related heart failure (14, 17). Here, we provide evidence that impaired AR receptor signaling caused by STAT3 deficiency leads to a higher secretion of PGD_2 by male but not female CKO-CM (Fig 7). PGD_2 subsequently impairs the vascular regeneration potential of CPC by inducing an epigenetic shift from endothelial to white adipocyte differentiation and thereby leads to a degradation of capillaries and an increase in WAT deposits in hearts from aging male but not female CKO mice (Fig 7). These data shed light on sex-specific age-related remodeling processes that contribute to age-related heart failure in males.

PGD_2 is generated by multiple enzymatic steps from arachidonic acid and COX-2 is a rate limiting enzyme in this process (34). COX-2 is elevated in CM from female and male CKO mice, an observation that contrasts with findings showing that STAT3 is a direct transcription factor of COX-2 in ischemic preconditioning, where activation of cardiac STAT3 upregulates COX-2 in the heart (35). However, in our study with young male and female mice canonical STAT3 signaling is not activated suggesting that inactive STAT3 acts either directly or indirectly as a negative regulator of COX-2, a feature that will be explored in future studies. PGs are also regulated by the PG degrading enzyme HPGD (36) and here we observed lower expression of HPGD in male CKO-CM but not in female CKO-CM. In this context it has been shown that the AR can be activated by different ligands including interleukin (IL)-6 and testosterone (37). The AR is expressed in cardiomyocytes from various species including mouse and human (26, 38, 39) and STAT3 acts as a positive co-factor for AR signaling by directly interacting with amino acids 234-558 in the N-terminal domain of the AR (24). The AR is expressed on HL-1 cells and indeed, HPGD expression is lower in HL-1-STAT3-KD-CM compared to ctrl HL-1-CM. Moreover, testosterone induced a marked increase in HPGD in ctrl HL-1-CM, which was blunted in HL-1-STAT3-KD-CM supporting the notion that impaired AR-signaling under low STAT3 condition leads to lower expression of HPGD and with this explains

294 the sex-specific increase in PGD_2 secretion in male but not female cardiomyocytes from CKO
295 mice (Fig 7).
296
297 We demonstrated that PGD_2 is able to induce white adipocyte differentiation in WT-CPC. In
298 line with this effect of PGD_2, freshly isolated male CKO-CPC, if kept under the same cultivation
299 conditions, have an increased ability to differentiate into white adipocytes compared to age-
300 matched WT-CPC isolated from males. Furthermore, depending on the differentiation
301 conditions, clonally expanded CPC can differentiate into endothelial cells or into adipocytes
302 suggesting that not differences in the CPC populations but reduced STAT3 expression in
303 cardiomyocytes and subsequent PGD_2 secretion promotes the epigenetic shift in the
304 differentiation potential of CKO-CPC isolated from male CKO mice. Indeed, freshly isolated
305 CKO-CPC or PGD_2-treated WT-CPC displayed an increased production of the white adipocyte
306 differentiation factor ZFP423. ZFP423 is a transcription factor controlling preadipocyte
307 determination and maintenance of white adipocyte identity through suppression of the
308 thermogenic gene program (8, 10, 12, 40, 41). ZFP423 overexpression in cCPC was sufficient
309 to induce white adipocyte differentiation confirming the important role of ZFP423 for the
310 adipocyte commitment of CPC. Increased ZFP423 expression in male CKO-CPC was
311 associated with an upregulation of WAT markers (LYZ2, and Resistin) and either unchanged
312 expression (EBF2 and TMEM26) or no expression (PRDM16 and UCP1) of BAT/BET markers.
313 Finally, and in line with the sex-specific difference in PGD_2 production, CPC isolated from
314 female CKO hearts did neither exhibit increased ZFP423 expression nor enhanced adipocyte
315 differentiation.
316 BMP2, BMP4 and ZFP521 are known regulators of ZFP423 (30, 31) and ZFP521 suppresses
317 the adipocyte lineage by direct transcriptional repression of ZFP423 (42). In the present study,
318 expression of ZFP521, BMP2 and BMP4 were not altered in male CKO-hearts or in freshly
319 isolated male CKO-CPC compared with male WT hearts or WT-CPC, suggesting that these
320 factors are not responsible for the ZFP423 regulation in male CKO-CPC. In turn, PGD_2 and its
321 non-enzymatically generated metabolite 15-deoxy-delta(12,14)-prostaglandin-J_2 (PGJ_2) were

reported to decrease EZH2 mRNA and protein expression (43). EZH2 is a subunit of PRC2 and functions as a histone methyltransferase that is able to control CpG methylation through direct physical contact with DNA methyltransferases (DNMTs) (44). Reduced EZH2 levels in the *Zfp423* promoter are associated with lower histone and DNA methylation and higher expression of the *Zfp423* gene, which predisposes fetal progenitor cells to adipogenic differentiation (45). Indeed, in freshly isolated male CKO-CPC the EZH2 expression was reduced and several DMRs were hypomethylated in the *ZFP423* gene compared to male WT-CPC. Moreover, PGD_2 stimulation of WT-CPC reduced EZH2 expression and increased ZFP423 expression supporting the notion that PGD_2 alters the epigenetic signature of CPC towards adipocyte differentiation. This observation extends previous studies reporting that PGD_2 suppresses lipolysis in adipocytes and is associated with insulin resistance and body weight gain (46). This novel aspect of PGD_2 is interesting with regard to the controversial roles of PGD_2 documented for the cardiovascular system. In fact, it has been shown that PGD_2 has protective features for example in I/R injury (47) but may also have adverse effects, for example by inducing cardiomyocyte death (48) and/or vasoconstriction (49).

Beside the hypomethylated ZFP423 gene, male CKO-CPC displayed hypermethylated DMRs in genes promoting angiogenesis (e.g., *Epas1* and *Fgfr2* (28, 29)) consistent with their previously shown lower endothelial differentiation potential (22). Previous data showed that EPO secretion is reduced in the cardiac microenvironment from male CKO hearts and exogenous EPO restored the endothelial differentiation capacity in male CKO-CPC (22). The present study found that EPO reduced ZFP423 expression and adipocyte formation from CKO-CPC, suggesting that lower EPO levels in CKO hearts may further promote the shift from endothelial to adipocyte differentiation in CKO-CPC. So far, there is no evidence for a sex-specific regulation of EPO since EPO blood levels in patients undergoing androgen deprivation therapy remained unchanged (50).

Previous data reported reduced STAT3 in failing human hearts (15) and the present study reveals significantly lower HPGD expression in LV tissue from male patients with terminal heart failure. Furthermore, PGD_2 induced ZFP423 expression and adipocyte differentiation in human

iPSC. Therefore, a similar mechanism as described for male mice may also exists in humans and may explain sex-specific development of heart failure.

In conclusion, age-related reduction of cardiomyocyte STAT3 leads to impaired AR receptor signaling and subsequent reduced expression of the PG degrading enzyme HPGD (Fig 7). This results in an increased secretion of PGD_2 from cardiomyocytes in male but not female hearts (Fig 7). Subsequently, PGD_2 induces an epigenetic shift in CPC already prior to heart failure which hampers vascular regeneration and increases WAT deposits and thereby promotes adverse remodeling and heart failure (Fig 7).

Material and Methods

Unless otherwise stated, chemicals and reagents were all purchased from Sigma-Aldrich.

Animal experiments

Mice with a cardiomyocyte-restricted knockout of STAT3 (CKO: αMHC-Cre$^{tg/+}$; STAT3$^{flox/flox}$) and wildtype mice (WT: STAT3$^{flox/flox}$) were generated as previously described (17). Echocardiography was performed on 3- and 6-month-old, lightly sedated mice (isoflurane inhalation 0.5%) using a Vevo 770 (VisualSonics) as described (14).

All animal studies were conducted in accordance with the German animal protection law and with European Communities Council Directive 86/609/EEC and 2010/63/EU for the protection of animals used for experimental purposes. All experiments were approved by the Local Institutional Animal Care and Research Advisory Committee and permitted by the relevant local authority for animal protection.

Histology and immunostaining

For cardiac morphological analyses, hearts were embedded in Tissue Tek OCT and frozen at -80 °C. Interstitial collagen was analyzed in picro-sirius red F3BA-stained sections (17, 51). Inflammation was determined in LV cryosections with an antibody recognizing CD45 (BD Pharmingen 550539). Capillary density was determined in transversely sectioned LVs by isolectin B4 (Vector), counterstained with wheat germ agglutinin (WGA, Vector) and DAPI for nuclear stain (14, 51). For immunostainings using primary antibody recognizing Perilipin (#9349, Cell Signaling), Resistin (ab119501, abcam) or UCP1 (ab10983, abcam) cryosections were fixed in acetone, were washed 3 times with PBS and blocked with 10 % donkey serum and 0.3 % Triton in PBS for 1 h at room temperature. Cryosections were stained with Perilipin antibody (1:100), Resistin antibody (1:50) or UCP1 antibody (1:100) overnight at 4°C. Cryosections were washed 3 times and incubation with the secondary antibody Cy3-anti-rabbit (1:250, Jackson ImmunoResearch) and counterstaining with WGA was performed for 2 h at

388 room temperature. Nuclei were stained with DAPI Hoechst 33342 (Sigma-Aldrich). Images
389 were acquired with AxioVert200M microscope, Axiovison software 4.8, Axio Observer 7 and
390 Zen 2.6 pro software (Carl Zeiss) and with SP8 Leica Inverted confocal microscope.
391
392 **Isolation, characterization and culture of SCA-1$^+$ cardiac progenitor cells**
393 Isolation of SCA-1$^+$ cells from hearts of 3-month-old mice was performed as described
394 previously (22), and is described in detail in the supplemental methods.
395
396 **DNA Isolation for reduced representation bisulfite sequencing (RRBS)**
397 The DNA of freshly isolated CKO- and WT-CPC of 3-month-old male mice was prepared using
398 the DNeasy Blood and Tissue Kit according to the manufacturer's protocol (Qiagen).
399
400 **Reduced Representation Bisulfite Sequencing (RRBS)**
401 RRBS libraries for a total of n=6 samples (3 sample pools for CKO mice, 3 sample pools for
402 WT mice, 10-12 mice per pool) were prepared using the Ovation RRBS Methyl-Seq System
403 1-16 with TrueMethyl oxBS (NuGen), skipping the oxidation step but otherwise undertaken
404 according to manufacturer's instructions. The average conversion rate across all samples was
405 estimated to be 97 %. Sequencing was performed on a NextSeq500 instrument at the
406 Sequencing Core Facility of the Fritz-Lipmann-Institute Jena. The input DNA and concentration
407 used for library preparation are both given in S3 Table.
408
409 **Data analysis of RRBS**
410 *Preprocessing*
411 Sequencing yielded between 139M and 171M sequences (Table 1). After clipping using
412 *cutadapt* (52) (version 1.18; parameters --quality-cutoff 20 --overlap 5 --minimum-length 25 -u
413 7 -a AGATCGGAAGAGC), between 138M and 170M remained (Table 1). Before and after
414 clipping quality was inspected using *fastqc* (v0.11.5).
415 *Read alignment, conversion rates*
416 Using the Bisulfite Analysis Toolkit (BAT; v.0.1) (53-55), reads were aligned with *segemehl*

(v0.2.0) (53) to the Mus musculus reference genome GRChm38.p6 using standard parameters of the module 'BAT_calling' in mode '-F 1'. For the extraction of conversion rates, we used the module 'BAT_calling' with *haarz* (v0.1.7) (53, 55) and *samtools* (v1.6). The filtering of resulting vcf files containing the conversion rates was done using the module 'BAT_filter_vcf'. On average, mapping rates were ~89 % (S3 Table).

Calling of differentially methylated regions

The methylation data obtained from the previous step was summarized using 'BAT_summarize' after the adaptation of the source code to allow the processing of mice data (BAT_summarize_mouse). Specifically, the module was called by assigning all 3 WT samples to the control group and all 3 CKO samples to the case group (parameters --in1 Set1_WT_CPC.bedgraph, Set2_WT_CPC.bedgraph, Set3_WT_CPC.bedgraph --in2 Set1_CKO_CPC.bedgraph, Set2_CKO_CPC.bedgraph, Set3_CKO_CPC.bedgraph --groups control, case --h1 WT1, WT2, WT3 --h2 CKO1, CKO2, CKO3). The module was run with *circos* (56) (v0.69-6) and bedGraphToBigWig (v4). The calling of differentially methylated regions was carried out with 'BAT_DMRcalling' using *metilene* (v0.2-8; parameters -a control -b case -z "-m 3 -M 1000 -d 0.01 -v 0.0" -p 1 -d 0.01 -c 3) (57). In order to increase the sensitivity in the given setup, the minimum amount of CpGs per DMR was reduced to 3, and the distance between CpGs within one DMR was increased to 1kb. Subsequently, the raw *metilene* output was annotated with the extended ENSEMBL annotation for GRCm38.p6 (v.92) using *bedtools intersect* (v2.22.1) (58). For the extension of the gene annotation, all annotated genes were extended at their 5'-end by 5kb to include the promoter region.

Table 1. Read numbers and mapping statistics.

sample	raw reads	clipped reads	mapping
Set1 CKO	171274320	170175455	152837610 (89.81%)
Set1 WT	147258040	146432432	131141572 (89.56%)
Set2 CKO	143418782	142616983	127924806 (89.7%)
Set2 WT	139188392	138358371	123566916 (89.31%)

Set3 CKO	158225479	157255130	141428776 (89.94%)
Set3 WT	157426725	156389740	140337521 (89.74%)

A total of 5 DMRs with an FDR-adjusted p-value were reported. Due to the high homogeneity of the samples and the relatively small size, we decided to analyze two sets of regions filtered for two different unadjusted p-value criteria. The first set with a minimum group methylation difference 0.1 and $p<0.001$ yielded a total of 83 DMRs overlapping with 81 unique genes. To better inspect the CpG methylation within predicted DMRs (n=83), we calculated the median methylation for the respective DMRs for each sample (sFig. 1c) and visualized the data using R's pheatmap function (R version 3.4.1, pheatmap version 1.0.12) with standard parameters for clustering after centering and scaling in the row direction.

Sequencing data of the epigenetic analyses are available under accession number PRJNA602737 in the Sequence Read Archive. Due to the sample size and the exploratory nature of this exercise, we omitted the correction for multiple testing. Pooling the CpG methylation values for all 3 samples in the respective groups was used to confirm or reject methylation differences (Wilcoxon) in CKO-CPC compared with WT-CPC.

SCA-1$^+$ cell cloning

SCA-1$^+$ cell cloning was described previously (22, 32). The protocol for clonal expansion of CPC is given in the supplemental methods.

Retroviral-vector mediated expression of ZFP423

For retroviral-vector mediated expression of ZFP423 the pMSCVFLAG-ZFP423 was used (40). pMSCVFLAG-ZFP423 was a gift from Bruce Spiegelman (Addgene plasmid # 24764; RRID:Addgene_24764). The plasmid pMSCV-GFP was used for transduction of control cells. For generation of lentiviral supernatants, the ecotropic Phoenix Packaging cell line (kindly provided by G. Nolan, Stanford University, Stanford, CA, USA) was used (59). Briefly, $5x10^6$ Phoenix packaging cells were seeded on 10 cm plates in DMEM supplemented with 10 %

FBS. On the following day, retroviral constructs (5 µg), together with constructs encoding pGagpol (M57) (10 µg) and pEnv K73 (2 µg), were transiently transfected into Phoenix cells by the calcium phosphate transfection method. Six h after transfection, the media were replaced by DMEM supplemented with 10 % FBS and the cells were cultivated overnight. The media were removed and DMEM/F12 supplemented with 10 % FBS was added and further incubated for 24 h. Supernatants were harvested and filtered through a 40 µm nylon filter and were either directly used for the transduction of CPC or stored at -80 °C. Viral supernatants were added to CPC clones for 6 h in the presence of Polybrene (4 µg/ml). Transduction efficiency based on GFP-expression was controlled in all experiments.

Adipocyte differentiation of cCPC and isolated WT-CPC

For adipocyte differentiation, cCPC or isolated WT-CPC were seeded on 0.2 % gelatin in DMEM/F12 with 10 % FCS supplemented with ITS (10 µg/ml insulin, 5 µg/ml transferrin, 5 ng/ml sodium selenite), rhFGF-basic (10 ng/ml) and EGF (20 ng/ml). The medium was replaced every 2-3 days. Two days after confluence, adipocyte differentiation was induced in DMEM/F12 supplemented with 10 % fetal bovine serum, 1 µM dexamethasone (G-Biosciences), 0.5 mM methylisobutylxanthine, 1 µg/ml insulin and 1 % penicillin-streptomycin (Thermo Fisher Scientific). Indomethacin (100 µg/ml) or prostaglandin D_2 (1 µM) were added to the adipocyte differentiation medium. After 2 days, the adipocyte differentiation medium was removed and cells were maintained in DMEM/F12 supplemented with 10 % fetal bovine serum and 1 µg/ml insulin. The cells were harvested in TRIzol (Thermo Fisher Scientific) for RNA isolation or were fixed with 4 % paraformaldehyde for Oil Red O staining.

Information on stimulation of HL-1 cells are provided in the supplemental methods

Adipocyte differentiation of human iPSC

The protocols for the generation and for the adipocyte differentiation of human iPSC are given in the supplemental methods.

494

495 **Endothelial Differentiation of cCPC on matrigel**

496 The plates were coated with 50 µl/cm² Matrigel Basement Membrane Matrix (Corning) at 37 °C
497 for 30 min. Clonal CPC (50000 cells/cm²) were cultivated in EGM-2 complete medium (Lonza)
498 overnight. Cells were fixed using 4 % paraformaldehyde.

499

500 **Isolation of murine adult primary cardiomyocytes and cell culture**

501 Murine adult primary cardiomyocytes were isolated and cultivated as described previously (60)
502 from 3-month-old WT and CKO mice. Supernatants of adult primary cardiomyocytes were
503 collected after 48 h, centrifuged at 300xg for 10 min to deplete cell fragments and stored at -
504 80 °C. Cells were harvested in TRIzol (Thermo Fisher Scientific) for RNA isolation.

505

506 **Isolation of RNA and qRT-PCR**

507 Total RNA was isolated with TRIzol (Thermo Fisher Scientific) and cDNA synthesis was
508 performed as described previously (22). Real-time PCR with SYBR green dye method (Brilliant
509 SYBR Green Mastermix-Kit, Thermo Fisher Scientific) was performed with the AriaMx Real-
510 Time PCR System (Agilent Technologies) as described (22). Expression of mRNA levels were
511 normalized using the 2-ΔΔCT method relative to GAPDH or 18S. A list of qRT-PCR primers
512 used in this study is provided in the supplemental methods (sTab. 4, 5).

513

514 **Immunoblotting**

515 Immunoblots were performed according to standard procedures using SDS-PAGE (17) and
516 the STAT3-antibody (#9139, Cell Signaling),

517

518 **Flow Cytometry**

519 5*10⁵ freshly isolated CPC were stained with PREF-1 antibody (AF8277, R&D Systems) and
520 PDGFRα antibody (17-1401-81, eBioscience) for 15 min at room temperature. Flow cytometry
521 was performed using the FACSCalibur (BD Biosciences).

522

523 **Immunocytochemistry**

524 Immunostainings using isolectin B4 (Vector Laboratories) were performed according to
525 standard procedures (22). For immunostainings using primary antibody recognizing Perilipin
526 (#9349, Cell Signaling) or Resistin (ab119501, abcam) cells were washed 3 times with PBS
527 and blocked with 10 % donkey serum and 0.3 % Triton in PBS for 1 h at room temperature.
528 Cells were stained with Perilipin antibody (1:100) or Resistin antibody (1:50) overnight at 4°C.
529 Cells were washed 3 times and incubation with the secondary antibody Cy3-anti-rabbit (1:250,
530 Jackson ImmunoResearch) was performed for 2 h at room temperature. Nuclei were stained
531 with DAPI Hoechst 33342 (Sigma-Aldrich). Images were acquired with AxioVert200M
532 microscope and Axiovison software 4.8, Axio Observer 7 and Zen 2.6 pro software (Carl
533 Zeiss).

534

535 **Oil Red O staining**

536 Oil Red O staining was performed as previously described (22). A detailed description is
537 provided in the supplemental methods.

538

539 **Adipogenesis Detection Assay**

540 Triglyceride accumulation in LV heart tissue was quantified by an adipogenesis detection
541 assay (Abcam ab102513) according to the manufacturer's protocol.

542

543 **PGD_2 detection in supernatants of adult murine cardiomyocytes**

544 PGD_2 levels in the supernatants of primary adult murine cardiomyocytes were measured using
545 the prostaglandin D_2 ELISA kit (Cayman Chemicals No. 512031) according to the
546 manufacturer's protocols. PG levels in supernatants of primary adult murine cardiomyocytes
547 were normalized to the total RNA content of the cells.

548

549 **Patient Data**

550 LV tissues were taken from patients undergoing heart transplantation due to end-stage heart
551 failure caused by dilated (DCM) or ischemic (ICM) cardiomyopathy (DCM/ICM, n=8). LV tissue
552 from donor hearts not suited for transplantation served as controls (NF, n=6). The study was
553 approved by the MHH local ethic committee (Nr. 1833-2013).

554

555 **Statistical Analyses**

556 Statistical analysis was performed using GraphPad Prism version 5.0a and 8.1.2 for Mac OS
557 X (GraphPad Software, San Diego, CA, USA). Normal distribution was tested using the
558 D'Agostino normality test. Continuous data were expressed as mean ± SD. Comparison
559 between two groups was performed using one sample *t*-test or unpaired two-tailed t-test. When
560 comparing more than two groups, we used Bonferroni's multiple comparison test after one/two-
561 way ANOVA testing. A two-tailed *P* value of <0.05 was considered statistically significant.

562

563 ## Acknowledgements

564 We thank Martina Kasten, Silvia Gutzke, Birgit Brandt, Iris Dallmann and Tim Kohrn for
565 excellent technical assistance. We thank the research core unit for laser microscopy at the
566 Hannover Medical School and the Core Facility of the Fritz-Lipmann-Institute Jena.

567

568 ## Declaration of interest

569 None of the authors have any conflicts of interest or financial interests to declare.

570

571 ## Data availability

572 The array data of the epigenetic analyses are available under accession number
573 PRJNA602737 in the Sequence Read Archive (SRA).

574

575 ## Abbreviations

576 ANOVA, analysis of variance; AR, androgen receptor; ARVC, arrhythmogenic right ventricular
577 dysplasia; BAT, brown adipose tissue; BMP2, bone morphogenetic protein 2; BMP4, bone
578 morphogenetic protein 4; bpm, beats per minute; BW, body weight; CD, cluster of
579 differentiation; cDNA, complementary deoxyribonucleic acid; CEBPA, CCAAT/enhancer-
580 binding protein alpha; COX, cyclooxygenase; CPC, $Sca1^{+}$- cardiac progenitor cell; DCM,
581 dilated cardiomyopathy; DMEM, Dulbecco's Modified Eagle Medium; DMR, differentially
582 methylated region; EBF2, early B cell factor 2; EGF, epidermal growth factor; EGM-2,
583 endothelial cell growth medium-2; EPAS1, endothelial PAS domain protein 1; EPO,
584 erythropoietin; EPOR, erythropoietin receptor; EZH2, enhancer of zeste homolog 2; FABP4,
585 fatty acid binding protein 4; FCS, fetal calf serum; FGF, fibroblast growth factor; FGFR2,
586 fibroblast growth factor receptor 2; FITC, fluorescein isothiocyanate; FS, fractional shortening;
587 GLUT4, glucose transporter 4; HBSS, Hank's balanced salt solution; HPGD,
588 hydroxyprostaglandin-dehydrogenase-15; HW, heart weight; IB4, isolectin B4; ICM, ischemic
589 cardiomyopathy; i.p., intraperitoneal; ITS, insulin-transferrin, sodium selenite; LV, left ventricle;
590 LVEF, left ventricular ejection fraction; m, month; MACS, magnetic-activated cell sorting; MHC,
591 myosin heavy chain; mRNA, messenger ribonucleic acid; NaCl, sodium chloride; NF, non-
592 failing, PCR2, Polycomb repressive complexe 2; PDGFRα, platelet-derived growth factor
593 receptor alpha; PG, prostaglandin; PPARγ2, peroxisome proliferator-activated receptor
594 gamma isoform 2; PPCM, peripartum cardiomyopathy; PRDM16, PR-domain containing 16;
595 PREF-1, preadipocyte factor 1; qRT-PCR, quantitative real-time polymerase chain reaction;
596 rh, recombinant human; rmEPO, recombinant mouse erythropoietin; RRBS, reduced
597 representation bisulfite sequencing; Sca1, stem cell antigen-1; SD, standard deviation; SDS-
598 PAGE, sodium dodecyl sulfate polyacrylamide gel electrophoresis; STAT3, signal transducer
599 and activator of transcription 3; STAT3-KD, STAT3 knockdown; UCP-1, uncoupling protein-1;
600 UTR, untranslated region; WAT, white adipose tissue; WGA, wheat germ agglutinin; WT,
601 wildtype; Zfp423, zinc-finger protein 423, Zfp521, zinc-finger protein 521; ZNF, zinc nuclear
602 factor
603

604

References

1. Beale AL, Meyer P, Marwick TH, Lam CSP, Kaye DM. Sex Differences in Cardiovascular Pathophysiology: Why Women Are Overrepresented in Heart Failure With Preserved Ejection Fraction. Circulation. 2018;138(2):198-205.

2. Lam CSP, Arnott C, Beale AL, Chandramouli C, Hilfiker-Kleiner D, Kaye DM, et al. Sex differences in heart failure. Eur Heart J. 2019;40(47):3859-68c.

3. Karlsson T, Rask-Andersen M, Pan G, Hoglund J, Wadelius C, Ek WE, et al. Contribution of genetics to visceral adiposity and its relation to cardiovascular and metabolic disease. Nat Med. 2019;25(9):1390-5.

4. Anumonwo JMB, Herron T. Fatty Infiltration of the Myocardium and Arrhythmogenesis: Potential Cellular and Molecular Mechanisms. Front Physiol. 2018;9:2.

5. Godinez-Valdez VH, Cazares-Campos I, Aranda-Fraustro A, Lopez-Jimenez F, Cardenas M, Marquez MF. Cardiac rupture in a patient with an acute myocardial infarction and extensive fatty infiltration of the heart ("adipositas cordis"). Int J Cardiol. 2012;154(3):e62-4.

6. Lu M, Zhao S, Jiang S, Yin G, Wang C, Zhang Y, et al. Fat deposition in dilated cardiomyopathy assessed by CMR. JACC Cardiovasc Imaging. 2013;6(8):889-98.

7. Rui L. Brown and Beige Adipose Tissues in Health and Disease. Compr Physiol. 2017;7(4):1281-306.

8. Shao M, Gupta RK. Transcriptional brakes on the road to adipocyte thermogenesis. Biochim Biophys Acta Mol Cell Biol Lipids. 2019;1864(1):20-8.

9. Shapira SN, Seale P. Transcriptional Control of Brown and Beige Fat Development and Function. Obesity (Silver Spring). 2019;27(1):13-21.

10. Aldiss P, Davies G, Woods R, Budge H, Sacks HS, Symonds ME. 'Browning' the cardiac and peri-vascular adipose tissues to modulate cardiovascular risk. Int J Cardiol. 2017;228:265-74.

631 11. Shao M, Ishibashi J, Kusminski CM, Wang QA, Hepler C, Vishvanath L, et al. Zfp423
632 Maintains White Adipocyte Identity through Suppression of the Beige Cell Thermogenic
633 Gene Program. Cell metabolism. 2016;23(6):1167-84.
634 12. Conte M, Martucci M, Sandri M, Franceschi C, Salvioli S. The Dual Role of the
635 Pervasive "Fattish" Tissue Remodeling With Age. Front Endocrinol (Lausanne). 2019;10:114.
636 13. Boengler K, Buechert A, Heinen Y, Roeskes C, Hilfiker-Kleiner D, Heusch G, et al.
637 Cardioprotection by Ischemic Postconditioning Is Lost in Aged and STAT3-Deficient Mice.
638 Circ Res. 2007;102(1):131-5.
639 14. Hilfiker-Kleiner D, Kaminski K, Podewski E, Bonda T, Schaefer A, Sliwa K, et al. A
640 Cathepsin D-Cleaved 16 kDa Form of Prolactin Mediates Postpartum Cardiomyopathy. Cell.
641 2007;128(3):589-600.
642 15. Podewski EK, Hilfiker-Kleiner D, Hilfiker A, Morawietz H, Lichtenberg A, Wollert KC,
643 et al. Alterations in Janus kinase (JAK)-signal transducers and activators of transcription
644 (STAT) signaling in patients with end-stage dilated cardiomyopathy. Circulation.
645 2003;107:798-802.
646 16. Stapel B, Kohlhaas M, Ricke-Hoch M, Haghikia A, Erschow S, Knuuti J, et al. Low
647 STAT3 expression sensitizes to toxic effects of beta-adrenergic receptor stimulation in
648 peripartum cardiomyopathy. Eur Heart J. 2017;38(5):349-61.
649 17. Hilfiker-Kleiner D, Hilfiker A, Fuchs M, Kaminski K, Schaefer A, Schieffer B, et al.
650 Signal transducer and activator of transcription 3 is required for myocardial capillary growth,
651 control of interstitial matrix deposition, and heart protection from ischemic injury. Circ Res.
652 2004;95(2):187-95.
653 18. Jacoby JJ, Kalinowski A, Liu MG, Zhang SS, Gao Q, Chai GX, et al. Cardiomyocyte-
654 restricted knockout of STAT3 results in higher sensitivity to inflammation, cardiac fibrosis,
655 and heart failure with advanced age. Proc Natl Acad Sci U S A. 2003;100(22):12929-34.
656 19. Lindner D, Hilbrandt M, Marggraf K, Becher PM, Hilfiker-Kleiner D, Klingel K, et al.
657 Protective Function of STAT3 in CVB3-Induced Myocarditis. Cardiol Res Pract.
658 2012;2012:437623.

659 20. Banerjee I, Fuseler JW, Intwala AR, Baudino TA. IL-6 loss causes ventricular
660 dysfunction, fibrosis, reduced capillary density, and dramatically alters the cell populations of
661 the developing and adult heart. Am J Physiol Heart Circ Physiol. 2009;296(5):H1694-704.
662 21. Haghikia A, Missol-Kolka E, Tsikas D, Venturini L, Brundiers S, Castoldi M, et al.
663 Signal transducer and activator of transcription 3-mediated regulation of miR-199a-5p links
664 cardiomyocyte and endothelial cell function in the heart: a key role for ubiquitin-conjugating
665 enzymes. Eur Heart J. 2011;32(10):1287-97.
666 22. Hoch M, Fischer P, Stapel B, Missol-Kolka E, Sekkali B, Scherr M, et al.
667 Erythropoietin preserves the endothelial differentiation capacity of cardiac progenitor cells
668 and reduces heart failure during anticancer therapies. Cell Stem Cell. 2011;9(2):131-43.
669 23. Zhang W, Qu X, Chen B, Snyder M, Wang M, Li B, et al. Critical Roles of STAT3 in
670 beta-Adrenergic Functions in the Heart. Circulation. 2016;133(1):48-61.
671 24. Ueda T, Bruchovsky N, Sadar MD. Activation of the androgen receptor N-terminal
672 domain by interleukin-6 via MAPK and STAT3 signal transduction pathways. J Biol Chem.
673 2002;277(9):7076-85.
674 25. Signaroldi E, Laise P, Cristofanon S, Brancaccio A, Reisoli E, Atashpaz S, et al.
675 Polycomb dysregulation in gliomagenesis targets a Zfp423-dependent differentiation
676 network. Nature communications. 2016;7:10753.
677 26. Kim TH, Park JM, Kim MY, Ahn YH. The role of CREB3L4 in the proliferation of
678 prostate cancer cells. Sci Rep. 2017;7:45300.
679 27. Shen JS, Meng XL, Wight-Carter M, Day TS, Goetsch SC, Forni S, et al. Blocking
680 hyperactive androgen receptor signaling ameliorates cardiac and renal hypertrophy in Fabry
681 mice. Hum Mol Genet. 2015;24(11):3181-91.
682 28. Matsunaga S, Okigaki M, Takeda M, Matsui A, Honsho S, Katsume A, et al.
683 Endothelium-targeted overexpression of constitutively active FGF receptor induces
684 cardioprotection in mice myocardial infarction. J Mol Cell Cardiol. 2009;46(5):663-73.

685 29. Takeda N, Maemura K, Imai Y, Harada T, Kawanami D, Nojiri T, et al. Endothelial
686 PAS domain protein 1 gene promotes angiogenesis through the transactivation of both
687 vascular endothelial growth factor and its receptor, Flt-1. Circ Res. 2004;95(2):146-53.
688 30. Addison WN, Fu MM, Yang HX, Lin Z, Nagano K, Gori F, et al. Direct transcriptional
689 repression of Zfp423 by Zfp521 mediates a bone morphogenic protein-dependent osteoblast
690 versus adipocyte lineage commitment switch. Mol Cell Biol. 2014;34(16):3076-85.
691 31. Hammarstedt A, Hedjazifar S, Jenndahl L, Gogg S, Grunberg J, Gustafson B, et al.
692 WISP2 regulates preadipocyte commitment and PPARgamma activation by BMP4. Proc Natl
693 Acad Sci U S A. 2013;110(7):2563-8.
694 32. De Pauw A, Andre E, Sekkali B, Bouzin C, Esfahani H, Barbier N, et al. Dnmt3a-
695 mediated inhibition of Wnt in cardiac progenitor cells improves differentiation and remote
696 remodeling after infarction. JCI Insight. 2017;2(12).
697 33. Lehmann JM, Lenhard JM, Oliver BB, Ringold GM, Kliewer SA. Peroxisome
698 proliferator-activated receptors alpha and gamma are activated by indomethacin and other
699 non-steroidal anti-inflammatory drugs. J Biol Chem. 1997;272(6):3406-10.
700 34. Kochel TJ, Goloubeva OG, Fulton AM. Upregulation of Cyclooxygenase-
701 2/Prostaglandin E2 (COX-2/PGE2) Pathway Member Multiple Drug Resistance-Associated
702 Protein 4 (MRP4) and Downregulation of Prostaglandin Transporter (PGT) and 15-
703 Prostaglandin Dehydrogenase (15-PGDH) in Triple-Negative Breast Cancer. Breast Cancer
704 (Auckl). 2016;10:61-70.
705 35. Bolli R, Stein AB, Guo Y, Wang OL, Rokosh G, Dawn B, et al. A murine model of
706 inducible, cardiac-specific deletion of STAT3: its use to determine the role of STAT3 in the
707 upregulation of cardioprotective proteins by ischemic preconditioning. J Mol Cell Cardiol.
708 2011;50(4):589-97.
709 36. Wang W, Hu Y, Wang X, Wang Q, Deng H. ROS-Mediated 15-Hydroxyprostaglandin
710 Dehydrogenase Degradation via Cysteine Oxidation Promotes NAD(+)-Mediated Epithelial-
711 Mesenchymal Transition. Cell Chem Biol. 2018;25(3):255-61 e4.

712 37. Kanda T, Yokosuka O. The androgen receptor as an emerging target in
713 hepatocellular carcinoma. J Hepatocell Carcinoma. 2015;2:91-9.
714 38. Lonergan PE, Tindall DJ. Androgen receptor signaling in prostate cancer
715 development and progression. J Carcinog. 2011;10:20.
716 39. Vainio P, Gupta S, Ketola K, Mirtti T, Mpindi JP, Kohonen P, et al. Arachidonic acid
717 pathway members PLA2G7, HPGD, EPHX2, and CYP4F8 identified as putative novel
718 therapeutic targets in prostate cancer. Am J Pathol. 2011;178(2):525-36.
719 40. Gupta RK, Arany Z, Seale P, Mepani RJ, Ye L, Conroe HM, et al. Transcriptional
720 control of preadipocyte determination by Zfp423. Nature. 2010;464(7288):619-23.
721 41. Gupta RK, Mepani RJ, Kleiner S, Lo JC, Khandekar MJ, Cohen P, et al. Zfp423
722 expression identifies committed preadipocytes and localizes to adipose endothelial and
723 perivascular cells. Cell metabolism. 2012;15(2):230-9.
724 42. Addison WN, Hall KC, Kokabu S, Matsubara T, Fu MM, Gori F, et al. Zfp423
725 Regulates Skeletal Muscle Regeneration and Proliferation. Mol Cell Biol. 2019;39(8).
726 43. Pierron A, Le Pape E, Montaudie H, Castela E, De Donatis GM, Allegra M, et al.
727 PGJ2 restores RA sensitivity in melanoma cells by decreasing PRAME and EZH2. J
728 Dermatol Sci. 2014;73(3):258-61.
729 44. Vire E, Brenner C, Deplus R, Blanchon L, Fraga M, Didelot C, et al. The Polycomb
730 group protein EZH2 directly controls DNA methylation. Nature. 2006;439(7078):871-4.
731 45. Yang QY, Liang JF, Rogers CJ, Zhao JX, Zhu MJ, Du M. Maternal obesity induces
732 epigenetic modifications to facilitate Zfp423 expression and enhance adipogenic
733 differentiation in fetal mice. Diabetes. 2013;62(11):3727-35.
734 46. Fujimori K, Aritake K, Oishi Y, Nagata N, Maehara T, Lazarus M, et al. L-PGDS-
735 produced PGD2 in premature, but not in mature, adipocytes increases obesity and insulin
736 resistance. Sci Rep. 2019;9(1):1931.
737 47. Katsumata Y, Shinmura K, Sugiura Y, Tohyama S, Matsuhashi T, Ito H, et al.
738 Endogenous prostaglandin D2 and its metabolites protect the heart against ischemia-
739 reperfusion injury by activating Nrf2. Hypertension. 2014;63(1):80-7.

740 48. Koyani CN, Windischhofer W, Rossmann C, Jin G, Kickmaier S, Heinzel FR, et al. 15-
741 deoxy-Delta(1)(2),(1)(4)-PGJ(2) promotes inflammation and apoptosis in cardiomyocytes via
742 the DP2/MAPK/TNFalpha axis. Int J Cardiol. 2014;173(3):472-80.
743 49. Asirvatham-Jeyaraj N, Jones AD, Burnett R, Fink GD. Brain Prostaglandin D2
744 Increases Neurogenic Pressor Activity and Mean Arterial Pressure in Angiotensin II-Salt
745 Hypertensive Rats. Hypertension. 2019;74(6):1499-506.
746 50. Gagliano-Juca T, Pencina KM, Ganz T, Travison TG, Kantoff PW, Nguyen PL, et al.
747 Mechanisms responsible for reduced erythropoiesis during androgen deprivation therapy in
748 men with prostate cancer. Am J Physiol Endocrinol Metab. 2018;315(6):E1185-E93.
749 51. Hilfiker-Kleiner D, Shukla P, Klein G, Schaefer A, Stapel B, Hoch M, et al. Continuous
750 glycoprotein-130-mediated signal transducer and activator of transcription-3 activation
751 promotes inflammation, left ventricular rupture, and adverse outcome in subacute myocardial
752 infarction. Circulation. 2010;122(2):145-55.
753 52. Martin M. Cutadapt removes adapter sequences from high-throughput sequencing
754 reads. 2011. 2011;17(1):3.
755 53. Hoffmann S, Otto C, Kurtz S, Sharma CM, Khaitovich P, Vogel J, et al. Fast mapping
756 of short sequences with mismatches, insertions and deletions using index structures. PLoS
757 computational biology. 2009;5(9):e1000502.
758 54. Kretzmer H, Otto C, Hoffmann S. BAT: Bisulfite Analysis Toolkit: BAT is a toolkit to
759 analyze DNA methylation sequencing data accurately and reproducibly. It covers standard
760 processing and analysis steps from raw read mapping up to annotation data integration and
761 calculation of correlating DMRs. F1000Research. 2017;6:1490.
762 55. Otto C, Stadler PF, Hoffmann S. Fast and sensitive mapping of bisulfite-treated
763 sequencing data. Bioinformatics (Oxford, England). 2012;28(13):1698-704.
764 56. Krzywinski M, Schein J, Birol I, Connors J, Gascoyne R, Horsman D, et al. Circos: an
765 information aesthetic for comparative genomics. Genome research. 2009;19(9):1639-45.

766 57. Juhling F, Kretzmer H, Bernhart SH, Otto C, Stadler PF, Hoffmann S. metilene: fast
767 and sensitive calling of differentially methylated regions from bisulfite sequencing data.
768 Genome research. 2016;26(2):256-62.
769 58. Quinlan AR, Hall IM. BEDTools: a flexible suite of utilities for comparing genomic
770 features. Bioinformatics (Oxford, England). 2010;26(6):841-2.
771 59. Pear WS, Nolan GP, Scott ML, Baltimore D. Production of high-titer helper-free
772 retroviruses by transient transfection. Proc Natl Acad Sci U S A. 1993;90(18):8392-6.
773 60. Thackeray JT, Pietzsch S, Stapel B, Ricke-Hoch M, Lee CW, Bankstahl JP, et al.
774 Insulin supplementation attenuates cancer-induced cardiomyopathy and slows tumor disease
775 progression. JCI Insight. 2017;2(10).
776
777
778
779
780
781
782
783
784
785
786
787
788
789
790
791
792
793

794

795 # Figure Captions

796

797 **Fig 1. Male CKO mice with age-related heart failure display increased intraventricular**
798 **fat accumulation with enhanced inflammation and fibrosis.**
799 **(A)** Oil Red O staining of adipocytes in LV cryosections counterstained with hematoxylin of 3-
800 or 6-month-old (m) male WT or CKO mice, scale bars: 50 μm. **(B)** Bar graph summarizes the
801 number of adipocytes per section in 3- or 6-month-old male WT (3 m: n=6; 6 m: n=12) and
802 CKO (3 m: n=6; 6 m: n=7) LVs, *P<0.05 vs. WT 6 m, two-way ANOVA with Bonferroni's multiple
803 comparison test. **(C)** Immunofluorescence staining of Perilipin (red), Resistin (red) or UCP1
804 (red) counterstained with WGA-FITC (green) and DAPI (blue) in cryosections of heart tissue
805 (male 6 m CKO mice), scale bars: 25 μM. **(D)** Quantification of triglyceride content in LV
806 extracts from 6 m male WT (n=8) and CKO (n=7) mice, mean of WT was set at 100 %.
807 **(E)** Capillary density (upper panel: isolectin B4 (IB4, green)/WGA (red) and nuclear staining
808 DAPI (blue), CD45 positive infiltrates (middle panel: brown, co-stained with eosin) and Sirius
809 Red staining (lower panel) of LV cryosections of 6 m male WT or CKO mice, scale bars: 50 μm.
810 **(F)** Capillary density determined as the ratio of capillaries to cardiomyocytes in transversely
811 sectioned male WT (n=7) and CKO (n=5) LVs. **(G)** Dot plot summarizes ADGRE1 mRNA levels
812 of male WT (n=8) and CKO LVs (n=7), mean of WT was set at 100 %. **(H)** Quantification of
813 fibrosis from WT (n=6) and CKO (n=5) LVs in arbitrary units (arb. units). **(D-H)** All data are
814 mean±SD, *P<0.05, **P<0.01 vs. WT, two-tailed unpaired t-test.

815

816 **Fig 2. STAT3 deficiency alters COX-2 and HPGD expression in male cardiomyocytes**
817 **leading to increased prostaglandin D_2 levels.**
818 **(A, C)** Dot plots summarize mRNA levels of **(A)** HPGD and **(C)** COX-2 in LVs of 3-month-old
819 male WT (n=7) and CKO mice (n=8). **(B, D)** Dot plots summarize **(B)** HPGD and **(D)** COX-2
820 mRNA levels of WT- and CKO-cardiomyocytes (CM) isolated from 3-month old mice (n=6
821 animals per genotype). **(E)** Measurement of PGD_2 levels in supernatants of male WT- and

CKO-CM assessed by ELISA (n=6 animals per genotype), normalized to total RNA concentrations. **(F, G)** Bar graphs summarize mRNA levels assessed by qRT-PCR of **(F)** HPGD and **(G)** COX-2 in HL-1 cells treated with testosterone (10 nM) for 24 h. **(H)** Representative western blot showing protein expression of STAT3 in HL-1 control (ctrl) and STAT3-KD cells. Ponceau S (PS) served as a loading control. **(A-E)** All data are mean±SD, WT mean was set at 100 %, **P<0.01 vs. WT, two-tailed unpaired t tests. **(F-G)** Data are presented as mean±SD, n=4, mean of HL-1-ctrl PBS was set at 100 %, *P<0.05, **P<0.01 vs. HL-1-ctrl PBS, #P<0.05, ##P<0.01 vs. HL-1-STAT3-KD PBS, two-way ANOVA with Bonferroni's multiple comparison test.

Fig 3. PGD_2 promotes white adipocyte differentiation of male WT-CPC.

(A, B) Bar graphs summarize mRNA levels assessed by qRT-PCR of **(A)** EZH2 and **(B)** ZFP423 in WT-CPC after treatment with PGD_2 for 48 h. **(C)** Representative picture after Oil Red O staining of isolated WT-CPC treated with PGD_2 (1 µM) for 48 h and cultivated for 12 days, scale bars: 50 µm. **(D)** Relative quantification of Oil Red O measured by absorbance at 492 nm. **(E-J)** Bar graphs summarize mRNA levels assessed by qRT-PCR of **(E)** ZFP423, **(F)** PPARγ2, **(G)** CEBPA and **(H)** FABP4 in WT-CPC incubated with PGD_2 (1 µM) for 48 h and cultivated for 12 days. **(I-L)** Bar graphs summarize mRNA levels assessed by qRT-PCR of the white adipocyte markers **(I)** LYZ2 and **(J)** Resistin and of the brown/beige adipocyte markers **(K)** EBF2 and **(L)** TMEM26 in WT-CPC incubated with PGD_2 (1 µM). **(A, B, I-L)** Data are presented as mean±SD (WT-CPC isolated and pooled from 6 animals), mean of control cells was set to 100 %, *P<0.05, **P<0.01 vs. control, one sample t-test. **(E-H)** Data are presented as mean±SD (WT-CPC isolated and pooled from 3 animals), mean of control cells was set to 100 %, *P<0.05, **P<0.01 vs. control, one sample t-test.

Fig 4. Characterization and adipocyte formation of cultivated CPC isolated from young CKO and WT male mice with normal cardiac function.

(A) Flow cytometry (PDGFRα or PREF-1: black; IgG control: red) and **(B)** qRT-PCR analysis

of PDGFRα and PREF-1 in freshly isolated male WT-CPC, n=3 independent isolations (each isolation consists of 8-12 animals). The preadipocyte cell line 3T3-L1 served as a positive and GAPDH as a loading control. **(C)** IB4 staining of WT-CPC after 4 weeks in culture (IB4, green; DAPI, blue; scale bar: 100 μm). **(D)** Oil Red O staining visualizes spontaneous differentiation of adipocytes in WT- and CKO-CPC after 4 weeks of cultivation, scale bars: 50 μm. **(E)** Bar graph summarizing adipocyte counts of Oil Red O positive cells (n=5 independent isolations; each isolation consists of 10-12 animals per genotype). **(F-H)** QRT-PCR detects mRNA levels of adipocyte markers **(F)** CEBPA, **(G)** FABP4 and **(H)** ZFP423 after 4 weeks of cultivation in WT- and CKO-CPC (n=3, independent cell isolations; each isolation consists of 10-12 animals per genotype). **(I, J)** QRT-PCR detects mRNA levels of WAT markers **(I)** LYZ2 and **(J)** Resistin after *in vitro* cultivation in WT- and CKO-CPC (n=3 isolations per genotype). **(K, L)** QRT-PCR detects mRNA levels of BAT/BET markers **(K)** EBF2 and **(L)** TMEM26 after *in vitro* cultivation in WT- and CKO-CPC (n=3 isolations per genotype). **(E-L)** Bar graphs represent mean±SD, mean of WT was set at 100 %, *P<0.05, **P<0.01 vs. WT, one sample *t*-test.

Fig 5. Epigenetic analysis of freshly isolated CKO- and WT-CPC.

(A, B) Boxplots with single CpG methylation values for **(A)** *Epas1* (chr17:86759066-86759095) and **(B)** *Fgfr2* (chr7:130728553-130728597). **(C)** Boxplot with single CpG methylation values in a region overlapping with the 5'-UTR of exon 2 of *Zfp423* in CKO- and WT-CPC (chr8: 87783293-87783352). Each group contains 3 samples with methylation values for 6 CpGs within the indicated genomic interval, respectively (n=18). **(D)** Boxplot with single CpG methylation of a region approximately 1.5kb downstream of the second exon of *Zfp521* in CKO- and WT-CPC (chr18:13969640-13969667). For each of the 3 samples per group, 3 CpG methylation values in the identified region (n=9) are shown. **(E, F)** Bar graphs summarize mRNA levels detected by qRT-PCR of **E** ZFP423 and **F** ZFP521 in freshly isolated WT- and CKO-CPC (n=5 independent isolations, each isolation consists of 8-12 animals). **(G, H)** Dot plots summarize **(G)** BMP2 and **(H)** BMP4 mRNA levels of WT (n=7) and CKO (n=8) LVs. **(I)** Bar graph summarizes EZH2 mRNA levels detected by qRT-PCR in freshly isolated WT-

878 and CKO-CPC from 3-month-old male (n=5 independent isolations, each isolation consists of
879 8-12 animals). **(J, K)** Bar graphs summarize **(J)** EZH2 and **(K)** ZFP423 mRNA levels detected
880 by qRT-PCR in freshly isolated CPC from 3-month-old female WT and CKO mice (CPC
881 isolated and pooled from 3 WT and 2 CKO mice). **(A-D)** Differences in methylation values were
882 tested by Wilcoxon test, *P<0.05, **P<0.001. **(E-K)** Data are presented as mean±SD, mean of
883 WT was set to 100 %, *P<0.05 vs. control, **P<0.01 vs. control; (**E, F, J-K)** one sample *t*-test
884 and (**G, H)** two-tailed unpaired t test.
885
886 **Fig 6: Retroviral overexpression of ZFP423 leads to white adipocyte differentiation of**
887 **cCPC.**
888 **(A)** Oil Red O staining of cCPC with retrovirally-mediated overexpression of ZFP423. Control
889 cells were transduced with the pMSCV-GFP control virusplasmid, scale bars: 50 μm.
890 **(B)** Relative quantification of Oil Red O measured by absorbance at 492 nm. **(C-E)** QRT-PCR
891 detects mRNA levels of **(C)** ZFP423 and of the adipocyte markers **(D)** CEBPA and **(E)** PPARγ.
892 **(F, G)** qRT-PCR visualizes mRNA levels of the white adipocyte markers **(F)** LYZ2 and
893 **(G)** Resistin. **(H, I)** qRT-PCR visualizes mRNA levels of the brown/beige adipocyte markers
894 **(H)** EBF2 and **(I)** TMEM26. **(B-I)** Data are presented as mean±SD, mean of pMSCV-GFP
895 transduced control cells was set to 100 % (n=3 independent cell culture experiments), *P<0.05,
896 **P<0.01 vs. pMSCV-GFP transduced control cells, one sample *t*-test.
897
898 **Fig 7. Scheme explaining how cardiomyocyte STAT3-deficiency leads to enhanced**
899 **white adipocyte differentiation of CPC in male mice contributing to sex-specific cardiac**
900 **remodeling.**
901 The present scheme shows in the upper picture (Fig 7A) the WT male and in the lower picture
902 the CKO male cardiac signaling (Fig 7B). Sex-specific regulated pathways with dark red arrows
903 and sex-unspecific regulated pathways with black arrows. Cardiomyocyte (CM)-specific
904 deficiency of STAT3 (Fig 7B) leads to enhanced expression of COX-2 in male and female mice
905 whereas expression of HPGD is only reduced in male mice likely to result from impaired male-

specific hormonal-mediated AR signaling caused by the missing AR co-factor STAT3 in male CKO-CM. This results in increased secretion of PGD_2 and of its metabolite PGJ_2 only in male CKO-CM. Subsequently, elevated PGD_2 levels in the cardiac microenvironment reduced the expression of the EZH2 histone methyltransferase in CPC leading to reduced DNA methylation of its target gene *Zfp423* and with this to enhanced ZFP423 expression. ZFP423 promotes white and suppresses brown/beige adipocyte differentiation of CPC in male CKO hearts. Reduced secretion of EPO from CKO-CM lowers the endothelial differentiation potential of CPC (22) which is associated with hypermethylation of the angiogenic genes *Epas1* and *Fgfr2*. In addition, EPO restores endothelial differentiation and suppresses ZFP423 expression thereby attenuating the endothelial-to-adipocyte shift of CPC.

Supporting information

S1 Fig. Adipocyte formation in heart tissue of 3- and 6-month-old CKO mice and methylation analysis of freshly isolated CKO- and WT-CPC.

(A) Perilipin staining in LV cryosections of 3- and 6-month-old (m) WT or CKO female (f) mice, Perilipin (red), WGA (green) and DAPI (blue): scale bars: 50 μm**. (B)** Immunofluorescence staining of Perilipin (red), Resistin (red) or UCP1 (red) counterstained with WGA-FITC (green) and DAPI (blue) in cryosections of heart tissue (male 6 m CKO mice), scale: 25 μM.

S2 Fig. STAT3 deficiency alters COX-2 and HPGD expression in LVs of aged male CKO mice, whereas in females only COX-2 expression is altered resulting in no differences in secreted PGD_2 levels from isolated adult cardiomyocytes.

(A, E) Dot plots summarize mRNA levels of **(A)** HPGD and **(E)** COX-2 in LVs of 6-month-old male WT (n=8) and CKO mice (n=7). **(B, F)** Dot plots summarize mRNA levels of **(B)** HPGD and **(F)** COX-2 in LVs of 3-month-old female WT (n=7) and CKO mice (n=4). **(C, G)** Dot plots summarize mRNA levels of **(C)** HPGD and **(G)** COX-2 in LVs of 6-month-old female WT (n=6) and CKO mice (n=6). **(D, H)** Dot plots summarize **(D)** HPGD and **(H)** COX-2 mRNA levels of isolated adult female WT- and CKO-cardiomyocytes (CM) (CM isolated and pooled from 3 WT and 2 CKO mice). **(I)** Measurement of PGD_2 levels in supernatants of isolated adult female WT- and CKO-CM assessed by ELISA (CM isolated and pooled from 3 WT and 2 CKO mice), normalized to total RNA concentrations. **(J, K)** Bar graphs summarize mRNA levels assessed by qRT-PCR of **(J)** HPGD and **(K)** COX-2 in HL-1 cells treated with estrogen (10 nM) for 24 h. **(A-I)** All data are mean±SD, WT mean was set at 100 %, *P<0.05, **P<0.01 vs. WT, two-tailed unpaired t tests. **(J, K)** Data are presented as mean±SD, n=4, mean of HL-1-ctrl PBS was set at 100 %, *P<0.05, **P<0.01 vs. HL-1-ctrl PBS, two-way ANOVA with Bonferroni's multiple comparison test.

S3 Fig. PGD_2 treatment leads to white adipocyte differentiation of human iPSC.

(A) Oil Red O (red) and Resistin (red; DAPI (blue)) staining of PGD_2 treated human iPSC. **(B-**

946 **D)** Bar graphs summarize mRNA levels assessed by qRT-PCR of **(B)** EZH2**, (C)** ZNF423 and
947 **(D)** CEBPA of PGD_2 treated human iPSC (two iPSC clones were tested, n=3 independent cell
948 culture experiments for each clone). Bar graphs represent mean±SD, mean of control cells
949 was set at 100 %, *P<0.05, **P<0.01 vs. ctrl, one sample *t*-test.
950
951 **S4 Fig. Methylation analysis of freshly isolated CKO- and WT-CPC.**
952 **(A)** Heatmap of median methylation values in predicted DMRs (n=83) overlapping with
953 81 unique genes.
954
955 **S5 Fig. Adipocyte differentiation and endothelial cell formation of cCPC expanded from**
956 **single cells.**
957 **(A, B)** Differentiation of cCPC expanded from single cells **(A)** on Matrigel (left panel: phase
958 contrast, right panel: Isolectin B4 staining (green); scale bars indicate 100 μm) and **(B)** after
959 adipogenic induction (upper left panel: phase contrast; upper right panel: Perilipin staining
960 (red), nuclear staining, DAPI (blue); lower left panel: Oil Red O staining (red); and lower right
961 panel: Perilipin staining (green), nuclear staining, DAPI (blue), Oil Red O staining (red); scale
962 bars indicate 50 μm). **(C-J)** mRNA levels of progenitor cell markers (**(C)** SCA1 and **(D)**
963 PDGFRα), general adipocyte markers (**(E)** CEBPA, **(F)** FABP4), WAT markers (**(G)** LYZ2,
964 **(H)** Resistin), and BAT/BET markers (**(I)** EBF2, **(J)** TMEM26) in undifferentiated and
965 differentiated cCPC (n≥4 independent cell culture experiments. Statistically significant
966 differences between the groups are represented as mean±SD, mean of mRNA expression
967 levels of undifferentiated cCPC were set at 100%, **P<0.01 vs. control, *P<0.05 vs. control,
968 one sample *t*-test).
969
970 **S6 Fig. EPO supplementation prevents enhanced adipocyte formation in cultivated male**
971 **CKO-CPC.**
972 **(A, B)** Bar graphs summarize ZFP423 mRNA levels in isolated male CPC incubated with
973 rmEPO (10 ng/ml) for **(A)** 48 h or **(B)** 4 weeks after isolation (**(A)**: n=3 cell isolations, each

974 isolation consists of 8-12 mice per genotype, **(B)**: n=5 independent isolations, each isolation
975 consists of 10-12 animals per genotype). **(C)** Oil Red O staining visualizes adipocytes in CKO-
976 CPC cultures after 4 weeks of cultivation with or without the addition of rmEPO (10 ng/ml),
977 scale bars: 50 μm. **(D)** Bar graph summarizing adipocyte counts (n=5 independent isolations,
978 each isolation consists of 10-12 animals per genotype). **(E, F)** qRT-PCR visualizes mRNA
979 levels of the adipocyte markers **(E)** CEBPA and **(F)** FABP4 after 4 weeks of cultivation (n=3
980 independent cell isolations, each isolation consists of 10-12 animals per genotype). **(G)** Bar
981 graphs summarize EZH2 mRNA levels in isolated CPC incubated with rmEPO (10 ng/ml) for
982 48 h (n=3 cell isolations, each isolation consists of 8-12 mice per genotype). **(A, B, D-G)** Data
983 are presented as mean±SD, mean of WT PBS was set at 100 %, *P<0.05, **P<0.01 vs. WT
984 PBS, #P<0.05, ##P<0.01 vs. CKO PBS, two-way ANOVA with Bonferroni's multiple comparison
985 test.
986
987

Fig 1

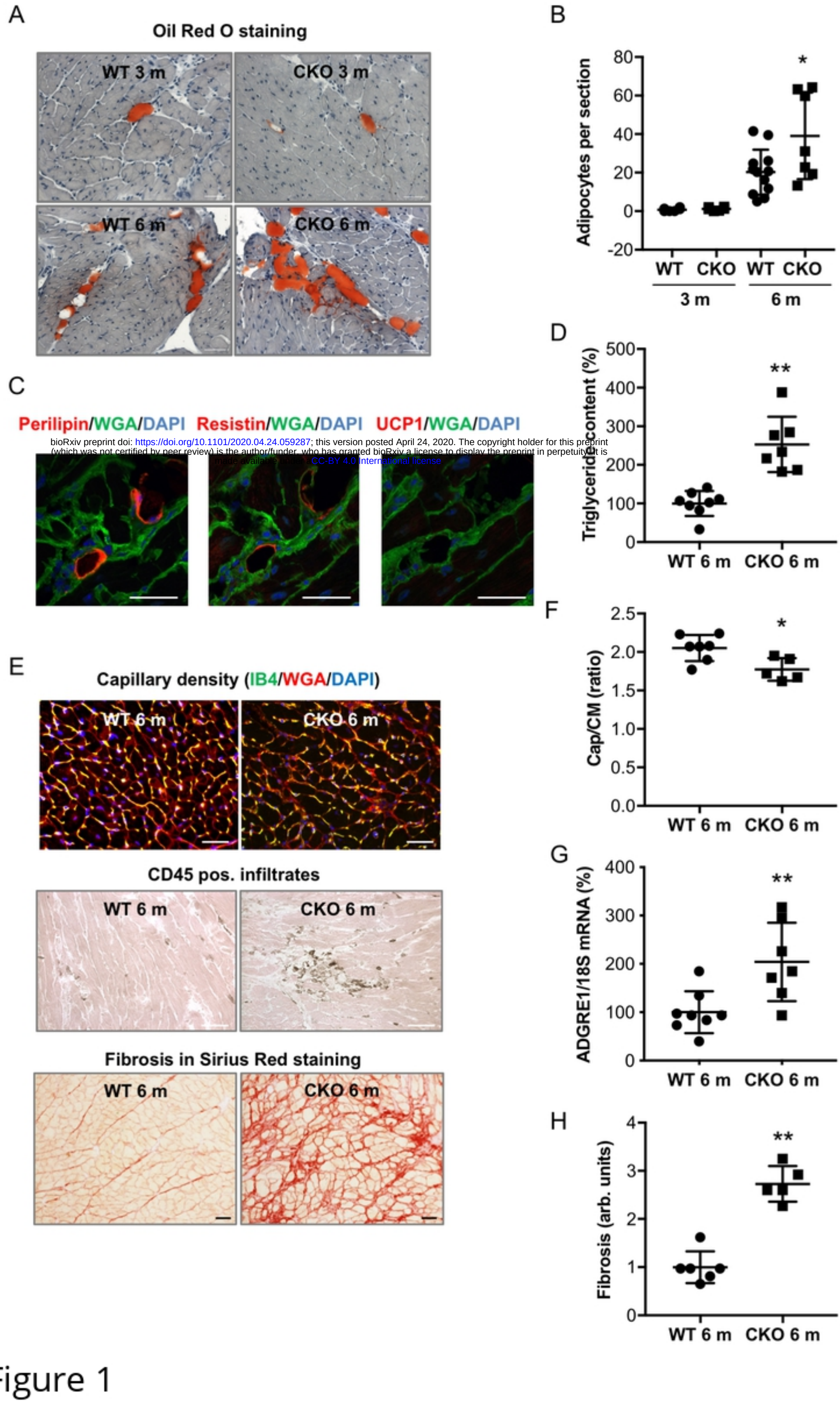

Figure 1

Fig 2

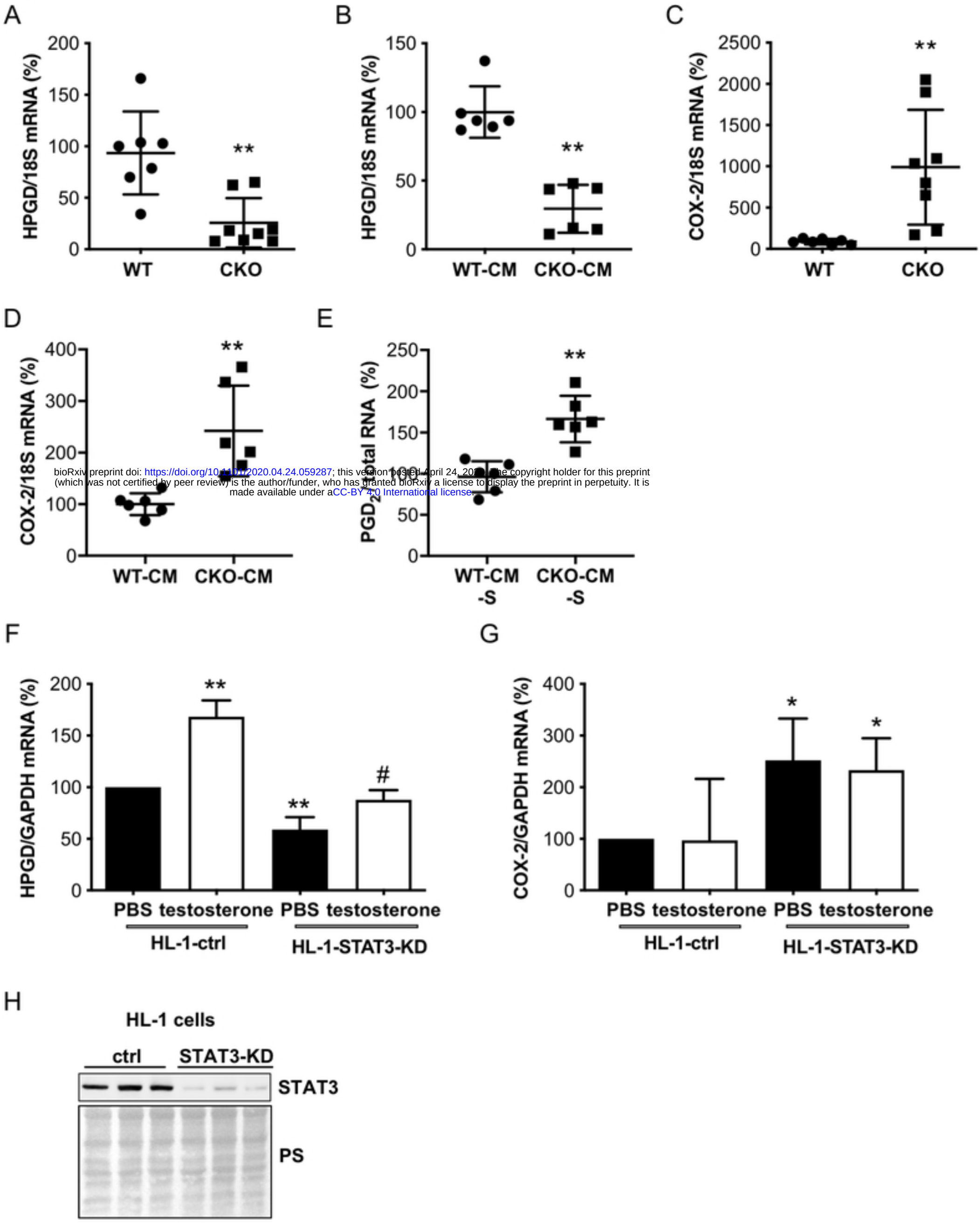

Figure 2

Fig 3

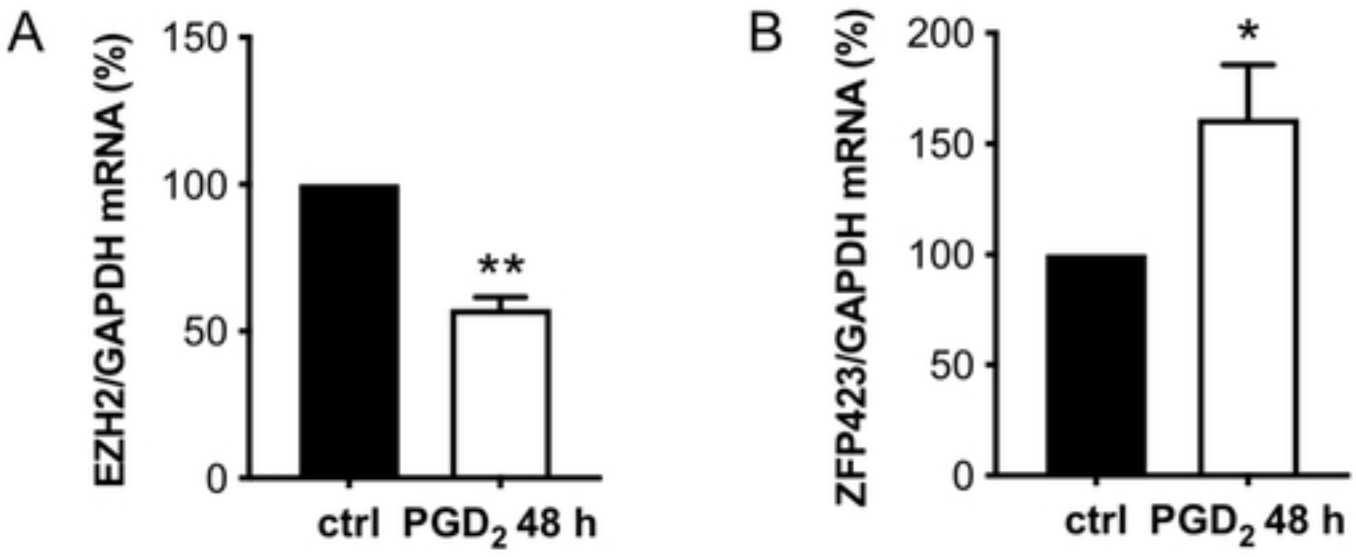

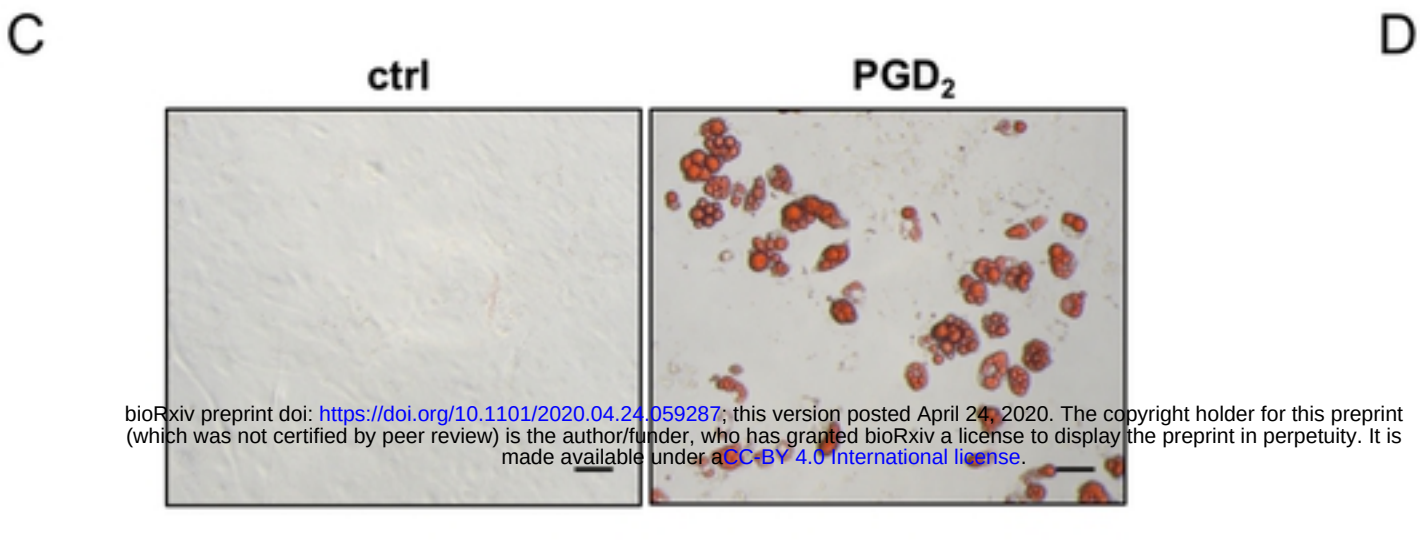

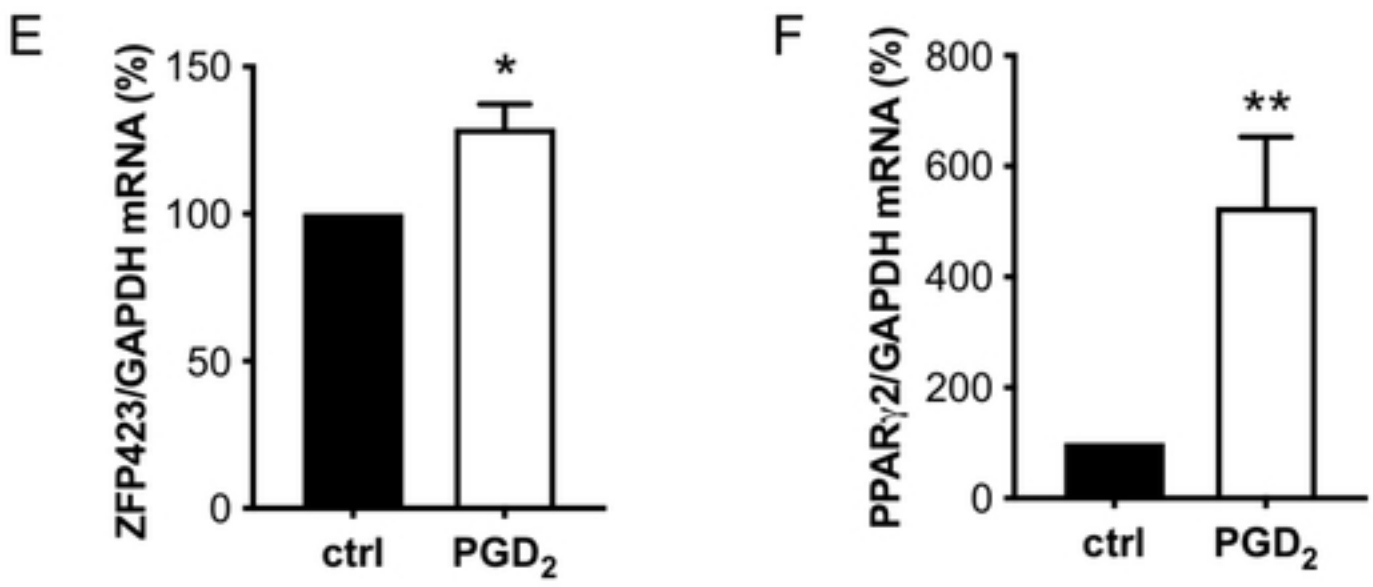

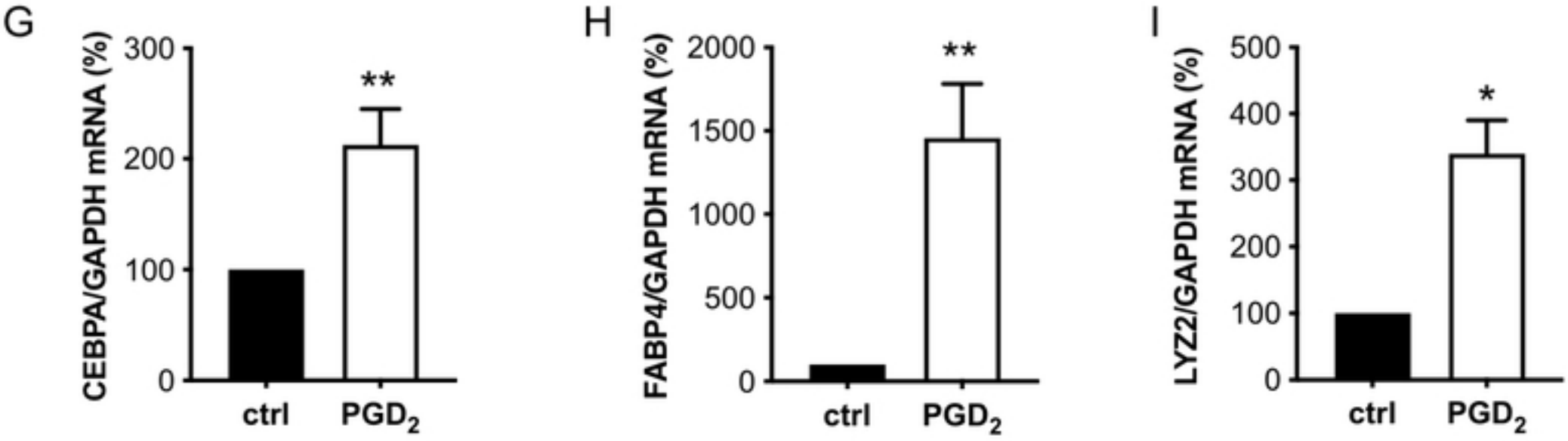

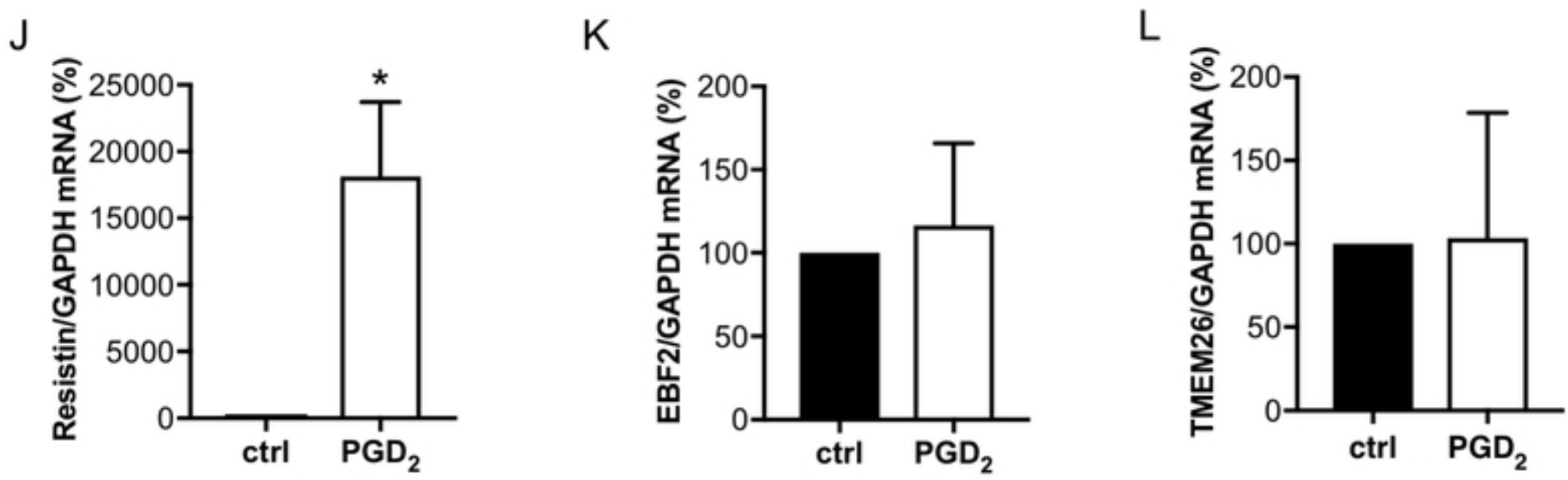

Figure 3

Fig 4

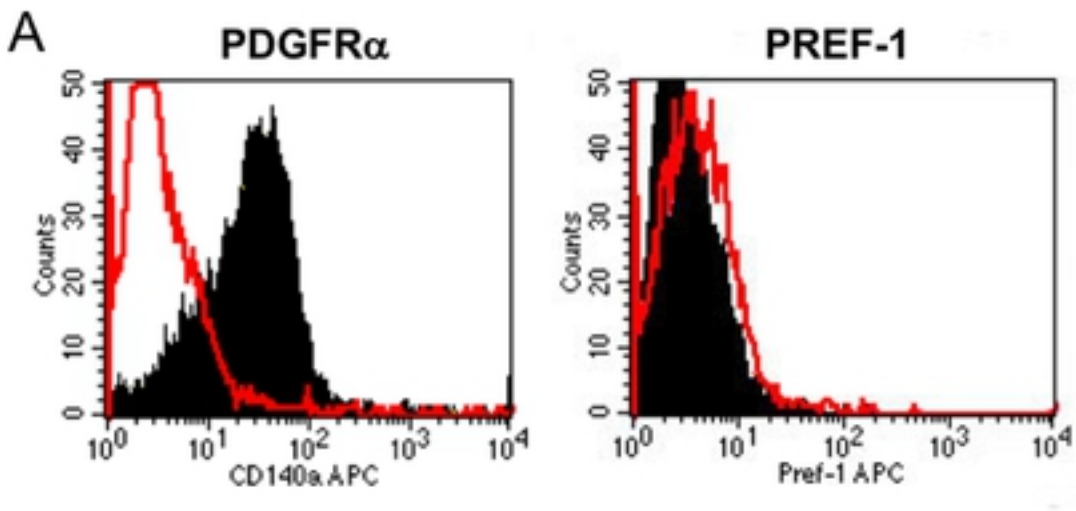

Figure 4

Fig 5

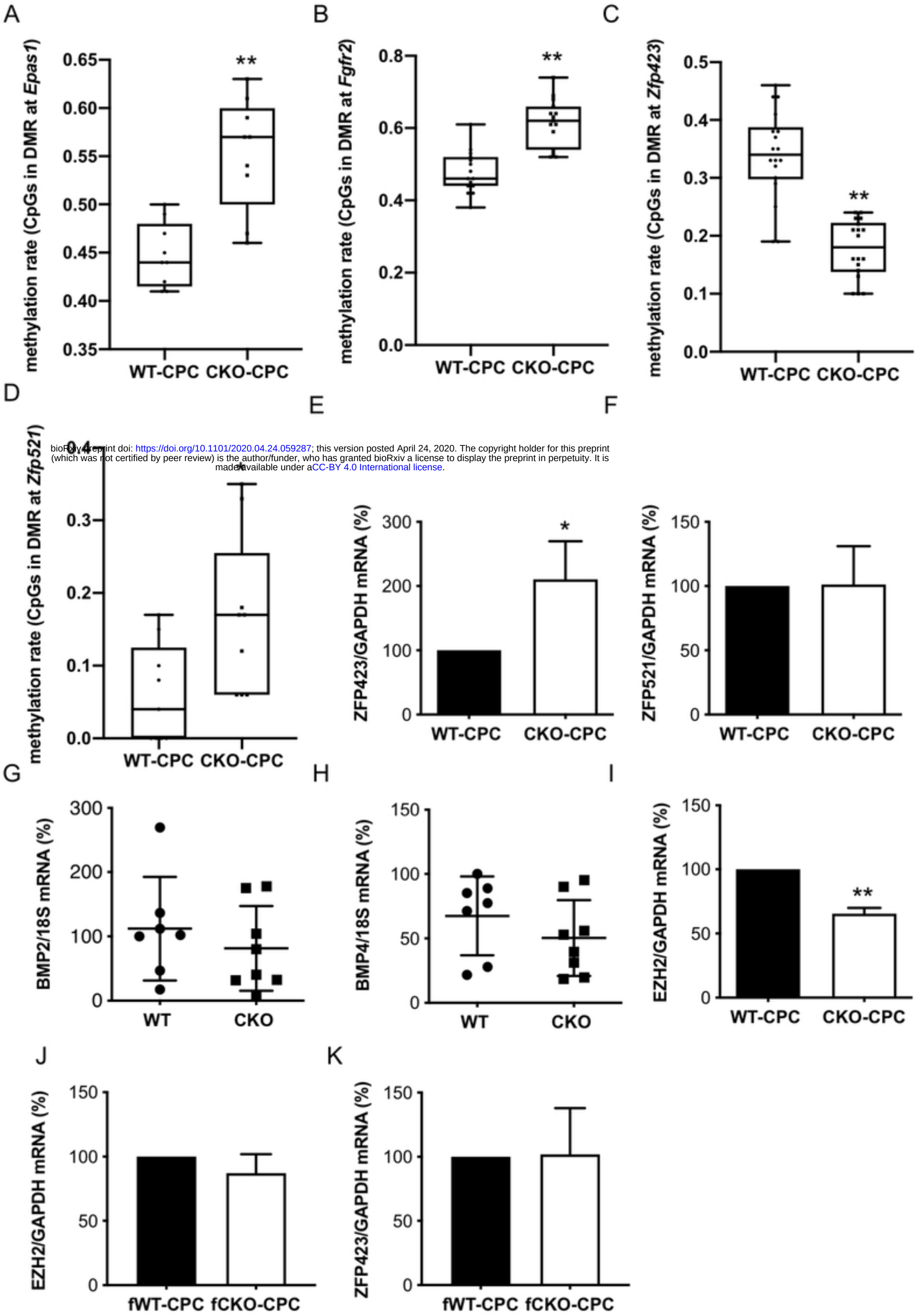

Figure 5

Fig 6

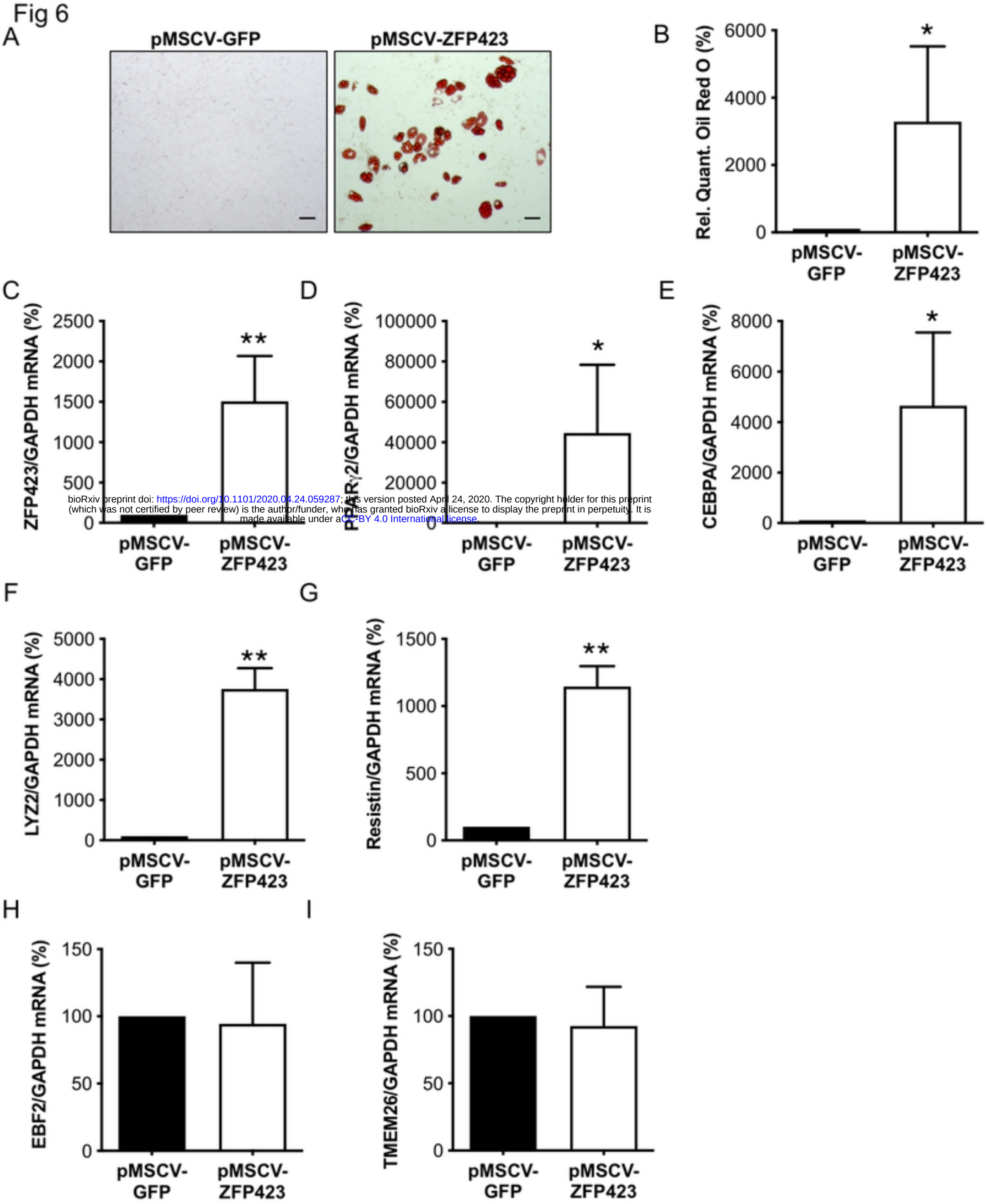

Figure 6

Fig 7A: **WT male**

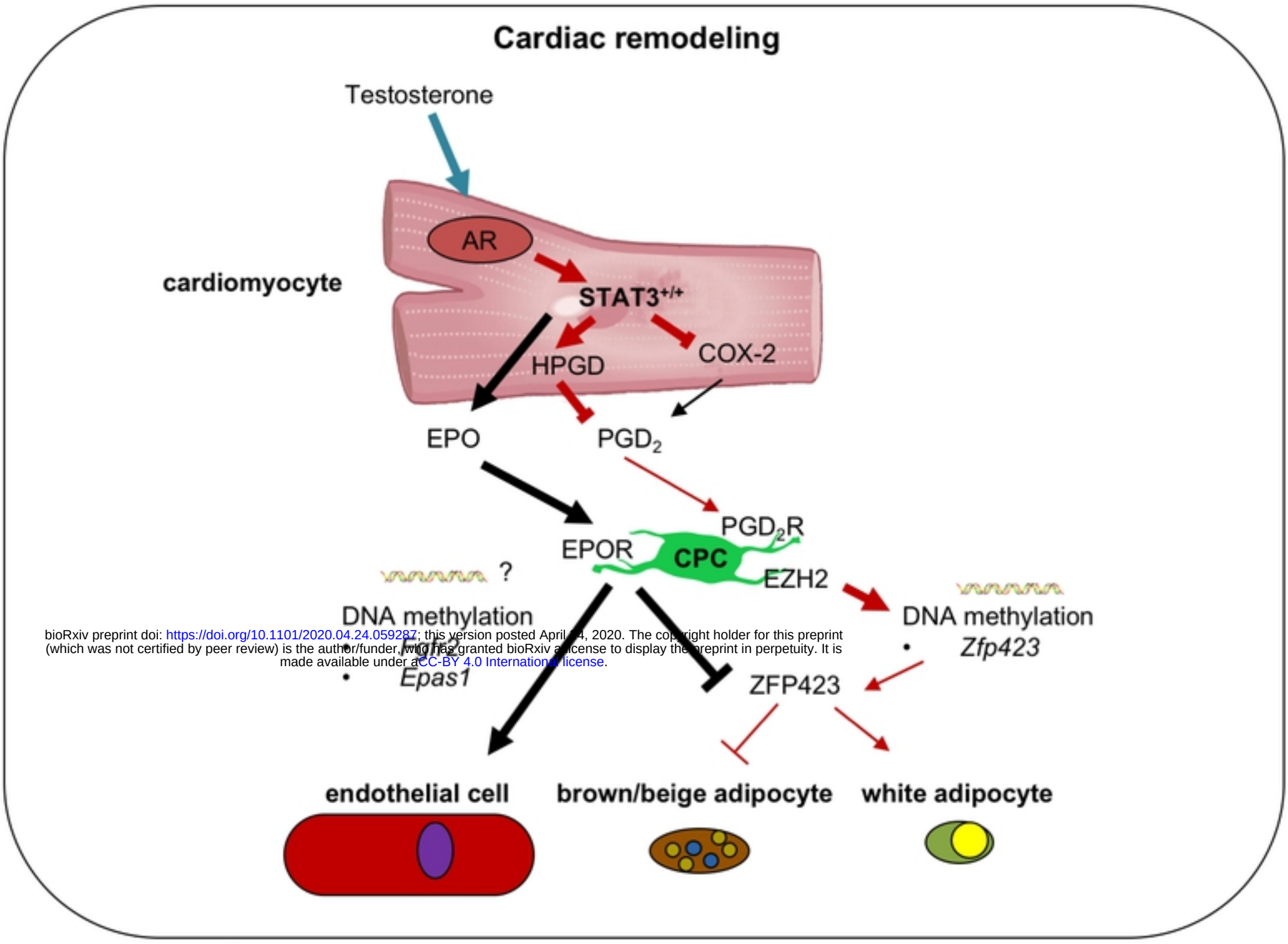

Fig 7B: **CKO male**

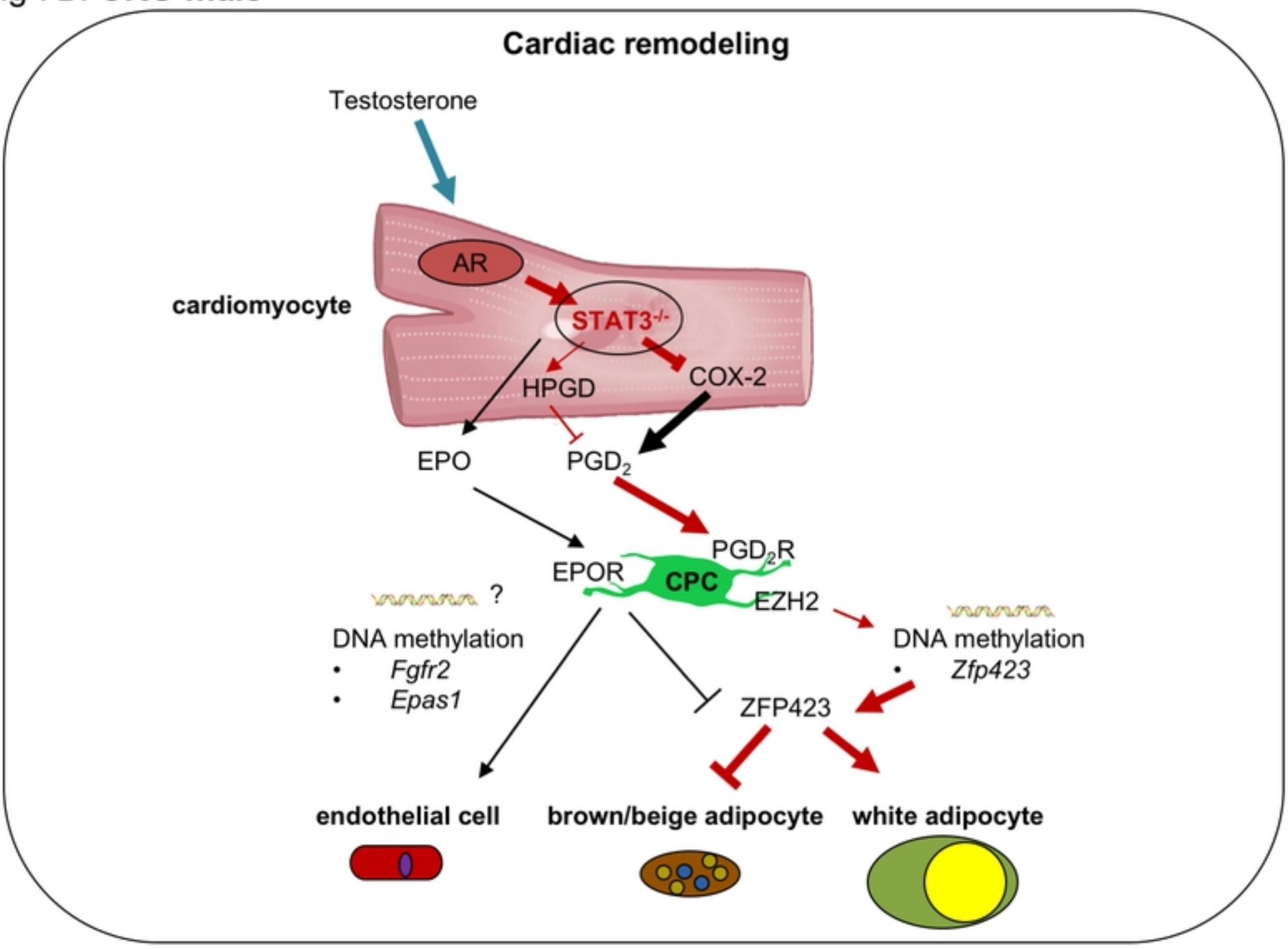

Figure 7